

...



THE UNIVERSITY
of EDINBURGH

BEng Mechanical Engineering Group Project

Metamaterial Based Continuously Variable Transmissions (CVT)

by

Khalid Alfawzan
Rodrigo Carnero Ibañez
Megan Hirst
Martin Starkov
Thomas Venter
Zalia Zainol

2022

Declaration

This project report is submitted in partial fulfillment of the requirements for the degree of BEng in Mechanical Engineering. We, Group 17, declare that this thesis was composed by ourselves, that the work contained therein is our own, except where explicitly stated otherwise in the text, and that it has not been submitted, in whole or in part, for any other degree or professional qualification.

Word Count: thesis

This thesis was conducted under the supervision of Dr Parvez Alam.

Abstract

Continuously variable transmission (CVT) gear systems are ubiquitous in industries where seamless torque transitions are a requirement. Despite this and their improved efficiency over other gearing systems, a big hurdle preventing the wider adoption of CVT systems has been their large space requirement. Furthermore, the fundamental operating mechanisms of pulley-based CVT systems have not been innovated upon significantly since their inception. This thesis discusses and demonstrates how the application of shape morphing meta-structures can be utilized in CVT gear systems to save space. Traditionally, their expansion and contraction is based on the push-pull of conical pulleys which compress a central belt, changing its radial diameter and hence gear ratio. These mechanisms often occupy a large amount of space in the axial direction. The question is therefore raised: can a 2-dimensional form of expansion replace traditional conical pulleys? Two mechanisms for planar expansion are explored: the expanding pulley and the Hoberman ring. The expanding pulley is a common approach for the radial expansion of gears. Meanwhile, the Hoberman ring meta-structure, which employs a repeating scissor pattern, is novel in this application. These two options are first reviewed in the context of relevant scientific literature, wherein their feasibility is validated. Following this, parametric analysis is employed alongside numerical simulations to design, assemble, and test two small-scale prototypes. A TRL4 level Hoberman ring CVT system was constructed, achieving an axial space reduction of 15.5%. The final assembly used two inversely spinning servos which expanded the ring for a continuous gear ratio from 2:1 up to 1:2. However, it was unable to spin and transmit power due to rotational actuation. Future design changes such as linear actuation combined with a bell-crank are briefly explored as the next stages in this research. The expanding pulley model, on the other hand, was found to have space saving of up to 86% in the axial direction and theoretical gear ratios from about 8:1 up to 1:8, though only a TRL3 level was reached due to high friction in the manufactured prototype preventing actuation. Improvements in material selection for the expanding pulley could lead to a superior space saving design, due to its simplicity / low number of parts compared to the Hoberman ring.

Personal Statements

Khalid Alfawzan

In the Project, group members used my phone for audio recording for the pitch video shoot. Also, I provided the writing document as well as its layout, structure, and editing. I was responsible for merging the literature review from each group member in \LaTeX as well as merging the references in one ".bib" file. For the writing sections, I was in charge of the write-up of the Introduction Chapter 1, Conclusion Chapter 7, and the following sections: 4.6, 4.6.3, 4.7, 6.3. Lastly, I ordered some of the parts required for the completion of the manufacturing process.

Khalid Alfawzan

Rodrigo Carnero Ibañez

My intellectual contribution has been paramount for this project, from coming up with the idea of using meta-structures & the use of and expanding pulleys in CVTs. Furthermore, I contributed as the main actor in the pitch of the project. In addition, manufacturing of the Hoberman was undertaken by Martin & myself. Where I focused on the actuation which include, the developing the Arduino code and the design of the electrical circuit to control the Hoberman. Moreover, I undertook the theoretical calculations and theoretical modelling to determine dimensions of the Hoberman. I wrote the following sections: 2.3, 2.4, 4.1, 4.2 & Appendix B, D, E. Additionally, I was co-writer of sections: 6.1 & 6.2. I believe I was an active group member of the team and key to the success of the project.

A handwritten signature in black ink, appearing to read "Rodrigo Carnero Ibañez". The signature is fluid and cursive, with a long horizontal line extending from the end of the last name.

Megan Hirst

For this group project, I was involved in several aspects of its completion. I contributed to the planning & the initial iterations of the CAD designs of the expanding pulley. Additionally, I was responsible for reviewing & compiling literature about the types and applications of different actuation systems used in engineering & identifying how they might be applied to the project. I also contributed to the manufacture stage of the project by being present in the G.20 Mechanical Engineering Laboratory during the allocated sessions. I mainly assisted in preparing the pin joints for the Hoberman ring & laser cutting the parts for the expanding pulley. Finally, I was responsible for writing the following sections in the dissertation: 3.1, 3.4, 6.4 & 6.5. I believe that I was an active member of the group and made a positive and valuable contribution to the project as a whole.

MHirst

Martin Starkov

My contribution entailed the following: I was the director, creative mind, and sole editor behind the video pitch for the thesis. I spent more than 20 hours editing and changing the video to fit the creative vision of myself, the group, and the supervisory feedback. After this, I became the manufacturer of the Hoberman ring demonstrator which we used extensively in our presentation as well as being the backbone proof of concept to accept our thesis hypothesis. I modelled each part in CAD, iterated on the designs more than a hundred total times, set out a comprehensive manufacturing plan, printed / manufactured / assembled the majority of the prototype (95%+). I worked closely with Rodrigo on both testing and assembly once he integrated the electronics and code. I would estimate the total time commitment to the build process to be at least 50 hours of work (and 3 all-nighters). In addition to this, I contributed extensively to the writing of the thesis. I wrote the abstract, sections: 2.1, 2.1.1, 2.1.2, 2.1.3, 2.2.1, 6.1.3, A.4, and provided all the figures for the manufacturing section, as well as editing and reviewing the text in the majority of the thesis sections. I believe that without my contribution the project would have ended with a lesser video and presentation, as well as no physical prototype to support the hypothesis.

Martins

Thomas Venter

I was solely responsible for the simulations and geometric optimization is done within this report. I used SOLIDWORKS simulations to complete 67 individual simulations consisting of numerous components and over 44 hours of total runtime. I believe that without my

contribution the project would have ended with a lesser developed method and supported conclusion, as well as no simulation of the assembly to support the hypothesis. I did the research, implementation and justification for Design Philosophy, Results and Simulations which are sections. I completed the literature review of Meta structures and Shape Morphing properties of Metamaterials which was in section 2.4.4, which Rodrigo and I peer reviewed. I assisted in the planning and co-created the writing plan as well. I supplied the template for the presentation and thoroughly enjoyed the entire process. I truly believe my intellectual contribution was critical to the success of the project and I believe I was a active and enthusiastic team member.



Zalia Zainol

Throughout this group project, I was the main person who set up the meetings and record all the meeting minutes which can be found in teams. Other than that, I was the main person in charge of designing the expanding pulley from the first sketch made on OnShape until the manufacturing and assembling bit of the expanding pulley in the G20 Lab. I went through a lot of iterations modelling each part of the expanding pulley on OnShape and came out with the calculations and dimensions necessary to achieve the final design. I did all the write ups in the report regarding the expanding pulley which are Section 4.3, 4.4, 4.6.2, 6.1.4, 6.2, A.5, A.6, C and the bill of materials in Appendix F. For the literature review, I wrote on material selections, Section 2.2 which explores the ideal material that can be used in designing the CVT.



Acknowledgements

We would like to express our gratitude to everyone who provided us with assistance and guidance throughout the project. The completion of this work would not have been possible without people such as Nicole Burg, Jonah Mack, and Sergio Miguez.

We are extremely grateful to our supervisor, Dr Parvez Alam, for his guidance and the knowledge and experience he shared with us. From the first meeting we had, he motivated, encouraged, and believed in us. Thank you Dr Parvez.

Contents

Declaration	i
Abstract	ii
Personal Statements	v
Acknowledgements	vi
List of Figures	x
List of Tables	xii
Abbreviations	xiii
1 Introduction	1
2 Literature Review	2
2.1 Continuously Variable Transmission Systems	2
2.1.1 Operating Principles	3
2.1.2 Current Applications	3
2.1.3 Belt Consideration	4
2.2 Materials	4
2.2.1 Polymer Choice for Prototyping	4
2.2.2 Material Properties	4
2.2.3 Belt Selection	5
2.3 Hoberman Structure and Its Geometry	5
2.4 Actuation Systems	7
2.4.1 Magnetic	7
2.4.2 Pneumatic	8
2.4.3 Thermal	9
2.4.4 Motorised	9
3 Design Philosophy	10
3.1 Metamaterial Applications in CVTs	10

3.2	Comparison Methods	12
3.3	Project Limitations	13
3.3.1	Budget	13
3.3.2	Equipment	13
3.3.3	Skills	14
3.3.4	Design Constraints	14
3.3.5	Time	14
3.4	Risks and Mitigation	15
4	Materials and Methods	16
4.1	Theory of Hoberman Ring	16
4.1.1	Scissor Pattern Derivation	16
4.1.2	Expanding Arms Derivation	19
4.1.3	Limiting Factors and Assumptions of the Hoberman	21
4.2	Iterative Design of the Hoberman	22
4.3	Theory of Expanding Pulley	23
4.3.1	Limiting Factors and Assumptions of the Expanding Pulley	24
4.4	Iterative Design of the Expanding Pulley	25
4.5	Simulations	27
4.5.1	Purpose and Theory	27
4.5.2	Types	27
4.5.3	Method and Scissor Arms as an Example	27
4.6	Manufacturing	29
4.6.1	Hoberman Ring	29
4.6.2	Expanding Pulley	32
4.6.3	Actuation	33
4.7	Experiments and Modelling	35
5	Results	36
5.1	Analysis of Method	36
5.1.1	Theoretical Analysis	36
5.2	Width and Volume Reduction	36
5.2.1	Simulations	37
6	Discussion	39
6.1	Improvements in our design	39
6.1.1	Hoberman Pushing Arms	39
6.1.2	Increasing the Hoberman Outer Ring Expansion Ratio	40
6.1.3	Rotation and Actuation	40
6.1.4	Expanding Pulley	42
6.2	Comparative Difference Between Conventional CVT, Hoberman, and Expanding Pulley	44

6.2.1	Expansion Ratio	44
6.2.2	Number of Parts	44
6.2.3	Width	44
6.3	Success Aspects	45
6.4	Further Applications of Meta-Structure CVTs	46
6.5	Alternative Methods for Proving the Hypothesis	46
7	Conclusion	47
References		48
A	Electronic Supplementary Material	51
A.1	Experimental Hoberman Videos	51
A.2	Hoberman Arduino Code	51
A.3	Simulation Supplementary material	51
A.4	Hoberman CAD Files	51
A.5	Experimental Expanding Pulley Videos	51
A.6	Expanding Pulley CAD Files	52
B	Hoberman Iteration Calculations	53
B.1	Iteration 1:	53
B.2	Iteration 2:	54
B.3	Iteration 3:	54
C	Expanding Pulley	56
C.1	Iteration 1:	56
C.2	Iteration 2:	56
C.3	Iteration 4:	56
D	Hoberman Arms Deflection Derivation	57
D.1	Vertical deflection of a half a circle	57
E	Arduino Circuit	60
E.1	Arduino Circuit Diagram	60
E.2	Potential Divider Circuit	61
F	Bill of Materials	62
G	Simulations	64

List of Figures

2.1	Operating principle of CVT	3
2.2	Hoberman scissor mechanism: expanded (right); collapsed (left) [1]	6
3.1	Traditional pulley-based CVT	11
4.1	Hoberman geometry at collapsed state	17
4.2	Trigonometric representation of Hoberman in collapsed state	17
4.3	Polygon angle theory to find α_{max}	18
4.4	Using trigonometry to find r_{inner}	18
4.5	Hoberman geometry at expanded state	19
4.6	Expanding arm stages. Left: contracted Hoberman; center: mid-expansion of Hoberman; right: fully expanded Hoberman	20
4.7	Expanding arm geometry	20
4.8	Parametric optimization of the scissor mechanisms accounting for physical dimensions [1]	21
4.9	Draft design of expanding pulley in contracted form	23
4.10	The two states of the expanding pulley	24
4.11	Conventional design of expanding pulley	24
4.12	Draft design of expanding pulley in contracted form	25
4.13	Labelled parts of the MG996R servo	25
4.14	Cutout of servo in the center of the lower arm	25
4.15	Cutout of the servo horn on the base of the upper arm	25
4.16	The servo-shaft coupler designed in OnShape	26
4.17	Servo-shaft coupler is used to connect the servo (left) and the shaft (right) .	26
4.18	Bearing is fitted in the center hole of the lower arm	26
4.19	Side view of the final design	26
4.20	Diagram showing the optimization process for each part	28
4.21	Diagram showing the failure of the scissor arm	29
4.22	Diagram showing the failure of the expansion arm	29
4.23	(a) Scissor pattern model (b) Endcap model (c) Manufactured scissor pattern	30
4.24	Loosely assembled Hoberman ring made of 8 scissor arm	30
4.25	Key Hoberman expansion mechanism parts	30

4.26	Central core with arms attached to it	31
4.27	Belt rail design	31
4.28	Plywood CAD model	32
4.29	The final Hoberman CVT system assembly	32
4.30	Manufactured expanding pulley parts in the lab	33
4.31	The upper arm, welded part, and screw positions	33
4.32	The Bluetooth application control panel	34
4.33	Hoberman expansion model	35
4.34	Expanding pulley expansion model	35
6.1	Straight expanding arms. Left image shows collision of the arms with the shaft at contracted state	40
6.2	Potential mechanism allowing simultaneous actuation and rotation of the Hoberman ring	41
6.3	Normal force, R exerted by the upper arm to the pulley	42
6.4	Hypothetical upper arm with linear arcs	43
D.1	Cross section of bent arm	58
D.2	FBD of bent arm	59
E.1	Arduino circuit diagram	60
E.2	Potential divider circuit	61

List of Tables

3.1	Limitations that influenced each task Red - Major Limitation, Orange - Minor Limitation, Green - Negligible limitation	14
3.2	Risks and mitigation	15
4.1	Dimensional iterations of the Hoberman	22
4.2	Dimensional iterations of the expanding pulley	27
4.3	Diagram showing the optimization parameters for scissor arms	28
4.4	Table showing the simulation outcome of optimization for the scissor arm . .	29
4.5	Angle and voltage mapping used in the actuation system	34
5.1	Results of simulations and geometric optimization	37
5.2	Qualitative results of the manufacturing process	37
6.1	Comparison between pulley-based CVT, Hoberman ring, and expanding pulley	45
F.1	Bill Of Materials (BOM)	63
G.1	Optimization outcomes based of iterations and requirements	65

Abbreviations

ABS Acrylonitrile Butadiene Styrene.

CAD Computer-Aided Design.

CVT Continuously Variable Transmission.

FDM Fused Deposition Modeling.

PETG Polyethylene Terephthalate Glycol.

PLA Polylactic Acid.

PTFE Polytetrafluoroethylene.

Note: Author abbreviations are shown in their corresponding reference entry.

Chapter 1

Introduction

Although continuously variable transmission (CVT) systems have been known for over 100 years, they only made their first appearance in the automotive industry 40 years ago when Subaru sold its first car in the United States that offered CVT as an option in the 1989 Justy GL automobile [2]. Since then, CVT systems have been widely studied and used in various applications. This is due to the advantages that CVT systems provide over manual and automatic transmissions. For example, CVTs allow for a smooth gear transition as well as low fuel consumption. Their working principle consists of two pulleys, primary and secondary, connected by a belt where the primary is linked to the engine and the secondary is connected to the gearbox. These pulleys are conical in shape and can take up a significant amount of space and weight, which are two major limitations of CVTs in most of their application fields [3]. In our project, the focus will be space reduction by means of an actuated meta-structure.

We hypothesize that the use of shape morphing meta-structures in CVT design will reduce their Euclidean space, specifically along the shaft axis.

The proposed structure, consisting of two Hoberman rings, which will expand and contract inversely to each other, hence changing the gear ratio between the input and output shafts. In addition, a modified version of an expanding pulley mechanism will be investigated as an additional space reduction alternative to the traditional CVT design. Traditional CVTs move a specialised power transmission belt radially outwards by pushing two conical pulleys against each other. This mechanism is bulky along the axis of rotation [3]. In contrast, the two proposed systems will expand their area using planar rotary actuation by means of servos. This will reduce space along the axis of rotation as the push-pull mechanism will be removed. Furthermore, calculations associated with the two proposed designs will demonstrate the theoretical viability of our proposals. An iterative approach will be used to optimise the design alongside static and kinematic simulations to support the theoretical calculations. After this iterative process, the two designs will be manufactured in the University of Edinburgh G.20 laboratory. This paper will discuss the simulation, design, and manufacturing processes behind the execution of a successful meta-structure based CVT system. Finally, future paths for the design will be explored as well as opportunities assessed for novel innovation by utilizing shape morphing meta-structures in CVTs.

Chapter 2

Literature Review

2.1 Continuously Variable Transmission Systems

CVTs have recently risen to prevalence in the automotive industry due to their improved fuel economy over traditional gear systems and their potential to reduce climate emissions [4]. Another application area of CVTs has been in small motor vehicles, such as snowmobiles. Continuous gear transitions in snowmobiles are imperative when navigating up steep hills [5]. The technology has also been applied in bicycle gearing, where it has been explored to improve efficiency and comfort of both professional and recreational cyclists. However, CVTs have not been widely adopted in bicycles due to their size and weight limitations [3]. This is one example of how innovation in CVT gear system technology, such as the size reduction explored in this thesis, could have widespread impact in industry.

Power transmissions are generally based on either belt drive connected pulleys or meshing gears. When exploring ways to reduce the size of power transmission systems, both types were investigated to see where improvements could be made via the use of shape morphing meta-structures. Meshing gear systems do not have an easily identifiable mode of bi-stability because the teeth of the gears only mesh when both gear modules match, and research on the topic is limited. Changing the size of a spur gear or any other toothed gear inherently changes the module unless a method for changing the number of teeth can be found [6]. Belt drive based systems, on the other hand, have already explored the concept of shape morphing via CVT technology. Thus, they lend themselves to improvement in this area using meta-structures.

2.1.1 Operating Principles

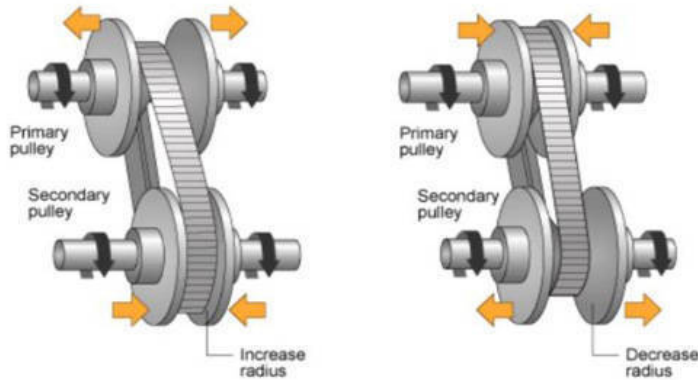


Figure 2.1: Operating principle of CVT

Traditional CVTs operate by connecting two cone shaped pulley pairs by a belt drive and pulling or pushing them together to change the radius of rotation around the shaft as seen in **Figure 2.1**. This has the effect of increasing or decreasing the gear ratio between the input and output shafts [7]. A fundamental part of this mechanism is the requirement to push and pull the pulleys along the shaft axis, which makes the system have a large footprint in all three spatial dimensions. Shape morphing meta-structure based CVTs could achieve the same efficiency benefits of traditional CVTs, while reducing the space required by utilising 2-dimensional expanding and contracting mechanisms, such as the Hoberman ring [8].

2.1.2 Current Applications

In an operating wind turbine, any variations in wind speed will cause a traditional gear system to switch gears, leading to a momentary discrete transition in rotation speed, seen as a frequency imbalance on the grid [9]. The lack of this discrete transition, alongside their improved efficiency, is an important factor for why CVTs have begun appearing in many power generation contexts, such as wind turbine power systems [10]. In addition to this, wind turbines strive to cause as little turbulence in their wake as possible, due to the phenomenon of wake-effect, which causes a reduction in the wind velocity of the air downstream of a wind turbine [11]. The proposed size reduction via a meta-structure would aid in making the gearing system more efficient while reducing the wake-effect.

In bicycles, achieving the greatest efficiency is of paramount importance as it directly impacts the effort required from the human operating it. CVTs fulfill this need well, but current designs are too bulky to be commercially viable. Shape morphing meta-structure CVTs offer the improvement of maintaining the desirable constant torque and performance of the CVT system while eliminating the requirement for axial movement of pulleys, which is a hindrance of the traditional CVT in the context of bicycles [3]. Furthermore, with

the meta-structure approach there is potential to create a system even thinner and more aerodynamic than the ubiquitous derailleur drive train mechanism.

2.1.3 Belt Consideration

Another aspect of traditional CVTs are the belts used to operate them. Currently, belt slippage against the conical pulley walls is a factor in the slow adoption of CVTs, as it can cause sudden unwanted deceleration, lowering the efficiency of the system [12]. The design proposed in this paper eliminates the need for an axially compressed belt, by allowing the belt to lay flat on the pulley, such as in flat belt drives which eliminates the risk of slippage.

2.2 Materials

2.2.1 Polymer Choice for Prototyping

In this thesis, part of the methodology involved manufacturing prototypes as proof of concepts to support the acceptance / rejection of the proposed hypothesis. When choosing a material for the prototypes, the primary consideration was its availability and ease-of-use in an iterative design process. Based on this, we explored ABS and PETG, and ultimately decided to use Polylactic Acid (PLA). This is a cheap and easily accessible plastic used in fused deposition modeling (FDM) 3D-printing [13]. Its widespread use meant that it was available in the laboratory environment provided to us as well as in one of our apartments. Alternative plastics such as ABS require well ventilated surroundings due to fumes, which would limit the environment in which we are able to manufacture. Additionally, PLA is recyclable, which makes it ideal for iterative design [14]. And most importantly, it had sufficient material properties for a small-scale TRL4 level prototype.

2.2.2 Material Properties

The main properties that are imperative in the prototype are its flexibility, strength and durability. Flexibility is needed to prevent the material from breaking as when the shape morphing mechanism is implemented, the gears are expected to expand and contract catering to different diameters. PLA is just as flexible as PETG whilst having higher strength and stiffness [15]. Even so, PETG has less scratch resistance making it a worse choice for printing gears [16]. When comparing PLA and ABS, their yield strength is 46.22 MPa and 61 MPa respectively [17]. ABS has better strength and resilience but it is not as flexible as PLA as the yield strength is higher. Due to its higher yield strength, ABS cannot withstand the same forces as PLA can without breaking [16]. PLA does not shrink when extruded, which is a weakness of ABS. Thus, with PLA, prints will be more accurate, more aesthetically pleasing, and more flexible [17]. PLA printed gears appear to be 12% more durable than those printed with ABS [18]. Besnea et al. [19] conducts a study regarding the wear of gearwheels manufactured through additive manufacturing. PLA, ABS, PETG, and nylon

are compared by testing each gearwheel for 3 hours in a clockwise direction and 3 hours in an anti-clockwise direction using a JGA 25-370 - 6V gearmotor with 58 rpm as the power source. From the test, PLA gears have been demonstrated to be the most effective in terms of wear, making them the most practical as intermediate gears in manufacturing processes. This supports the research conducted by Mert and Bekir [18]. Hence, PLA is chosen due to its convenience, excellent flexibility, weight, strength, durability, and wear characteristics.

2.2.3 Belt Selection

Conventional CVTs use stiff steel-reinforced V-belts. The V-belts use the compression of the moving pulleys to hold the belt up [13]. When the belt slips, there is no longer a link between the engine and transmission. The V-belt is what connects the primary clutch on the engine to the secondary clutch on the transmission. This slip is usually caused by a poor fit between the belt and the pulley. When this happens, the cost to repair the problem is high [13]. The tendency of conventional CVTs to need repairs owing to belt wear is one factor preventing them from hitting the mainstream market [20]. With the self-actuated morphing gears, we aim to increase the belt life as it is only in contact with the morphing gears along its circumference, not sides. By using a simple flat belt, we can reduce the weight of the whole CVT which contributes to the space reduction context while delivering the same performance as using a V-belt. Flat belt drives offer greater performance in terms of speed and are more cost-effective to adopt since they are simple, inexpensive, flexible, and durable [21]. Most flat belt drives that are used in machinery are made of flat leather, rubber and nylon belts. The material of choice for our belt must be low in cost and durable enough for a small-scale TRL4 level prototype. Based on this a natural rubber band was chosen.

2.3 Hoberman Structure and Its Geometry

Most of the literature in metamaterial actuation focuses on linear movements in one direction, such as the previously mentioned pneumatic caterpillar or the swimming frog actuated by a magnetic field. For expanding gears, there is a need for the expansion to be in the radial direction, ensuring a continuous ring during expansion / contraction. The paper by Chen et al. [1] addresses how the expansion of solar panels in space can be achieved using origami substrates actuated by temperature differentials in combination with a Hoberman ring mechanism. The Hoberman ring mechanism expands radially by several times its collapsed volume, always maintaining an almost perfectly circular shape through a scissor pattern architecture. This phenomena can be observed in **Figure 2.2** where the collapsed / contracted state is shown on the left and the expanded state on the right. The aforementioned paper investigates the geometry which provides the optimum expanded-collapsed area ratio. The expansion ratio depends on the number of scissor patterns pinned together and the maximum outer radius limited by the fabrication space. The greater the number of scissor patterns, the closer the polygon will assimilate to a perfect circle. Therefore, the

number of scissor patterns must be chosen to obtain the expanded radius. In the paper, it is stated that the maximum expansion ratio for a beam width of 4mm and 20 scissor patterns is:

$$\Delta A = \frac{A_{Expanded}}{A_{Collapsed}} = 11.99 \quad (2.1)$$

Additionally, the inner radius can be calculated using **Eq.2.2**. Where the collapsed area depends on the beam's width and the number of scissor patterns:

$$r_{inner} = \frac{1}{2} \cdot \omega \cdot \cot \frac{\pi}{2n} \quad (2.2)$$

Moreover, the paper analyses the limitation of the Hoberman mechanism. Theoretically, the Hoberman ring can have an infinite expansion-contraction ratio. The restriction comes from the width of the beams, which take up space when the Hoberman ring collapses. Hence, the larger the width, the higher the collapsed area, and the lower the expansion ratio. Therefore, having the thinnest width beam whilst also being able to withstand stress is imperative. The paper highlights the importance of getting this balance right to find the optimum expansion-contraction ratio. As stated previously, the other underlying limitation is the number of scissor patterns that can be physically fit in the available space. Overall, Chen et al.'s views on the Hoberman ring mechanism have convinced us that this is a viable design for the shape morphing gear system. Even considering its fabrication limitations, the Hoberman ring mechanism is the most efficient way of having continuous radial expansion whilst maintaining an almost perfect circular ring. Finally, the Hoberman ring is the mechanism that provides the most significant volume change from collapsed to expanded state [1].

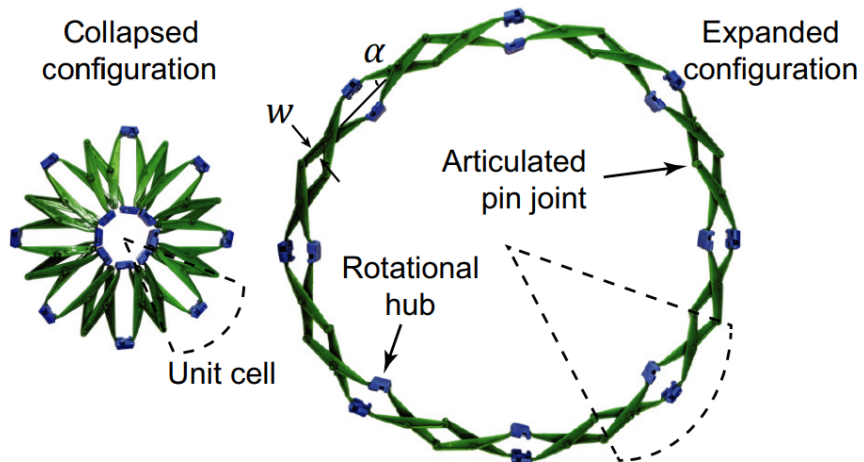


Figure 2.2: Hoberman scissor mechanism: expanded (right); collapsed (left) [1]

Although the Hoberman expansion ratio can be up to 12, there are limitations to it. These

limitations are highlighted by Maxime Daniel and Couture [22] in a paper about expandable illuminated rings. The paper highlights the maximum expansion ratio of the Hoberman when expanded using central pushing arms as $\Delta A = 4$. This is due to the limitation of the arms themselves which can only be expanded by the length of the radius in the inner circle. While this is a limiting factor, the mechanism lends itself to simple actuation via servos. Due the modular nature of the Hoberman ring, it was chosen as one of the primary demonstrator mechanisms in the prototypes of this project.

2.4 Actuation Systems

Actuation is the mechanism that converts energy into mechanical motion, causing a meta-structure to morph into a different shape. It is, thus, an important aspect of any shape morphing meta-structure.

We aim to find an actuation system that allows for a controllable circular expansion / contraction. Metamaterial actuation can be separated into three types of sub-groups: field-responsive material, soft mechanical actuation and soft electronics. [23] From our research, we have pinpointed the main actuation systems that can fit our proposed design to be magnetic, thermal, pneumatic, and motorised [24].

2.4.1 Magnetic

In Magnetic actuation, the idea is to apply stronger or weaker magnetic fields to morph the shape of the meta-structure. This solution provides high control and accuracy since the current in the electromagnet can easily control the magnetic field strength. Moreover, by inverting the current direction in the electromagnet, the direction of the magnetic field can be reversed; hence, the meta-structure can be quickly returned to its original position. The potential of this actuation system can be seen in the paper about symmetry breaking actuation by Wu [25], where beams are connected by a magnet to act as pin joints. The report highlights the use of a controlled magnetic field to simulate the movement of a frog in the water. The frog legs have three different positions when the legs produce negative thrust, which occurs when we apply a positive magnetic field. The legs produce positive thrust when we use a positive magnetic field. No magnetic field is applied when the legs glide. [25]

It is therefore clear how an electromagnetic field based actuation mechanism could be a viable solution to actuate our CVT system since it would enable the morphing of the circular gear by applying a positive magnetic field to repel the magnets and radially expand the gear. Similarly, an opposing magnetic field would attract the magnets towards the electromagnet to contract the gear. The paper shows more complex applications that display how the magnitude of the magnetic field can actuate different shapes in a metamaterial, which could be translated to the rate of expansion / contraction of the CVT meta-structure. The stronger the magnetic field, the faster the rate of contraction / expansion of the system. Other papers

by Xu and Lin [26] talk about the use of ferrite-based magnets in metamaterials to change the angle of a metamaterial to always face solar panels toward the light.

Although the literature has proved that using electromagnets in combination with ferrite-based magnets is a viable option for actuation systems, we have been unable to find any application of this actuation method on changing the distance between the electromagnet and magnets significantly. The applications reviewed in the literature always have one thing in common, the distance between the magnet and the electromagnet remains almost constant at any point of the actuation. An expanding CVT system would have the electromagnet at the centre of the gear and the magnet attached to the sides of the gear. As the gear expands, the distance between the magnet and the electromagnet would increase; hence the electromagnetic force the magnet would feel for a constant current through the electromagnet would decrease. This is explained by the inverse square law, which states that as the distance from the source increases, the field strength decreases, $B \propto \frac{1}{r^2}$. Hence, to keep the same rate of gear expansion, the current through the electromagnet would have to be increased exponentially (squared).

Therefore, the electromagnetic approach was discarded for an expanding gear actuation system.

2.4.2 Pneumatic

Pneumatic is one of the most common methods of actuating metamaterials. This works by using air pressure to morph a metamaterial into a different shape. A paper by Grossi et al. [27] investigates pneumatic actuation to mimic the movement of a caterpillar. The paper proposes using silicon blocks with air chambers that can be compressed or expanded by applying a negative or positive pressure gradients. When the edges of the silicon caterpillar expand, and the centre compresses, the caterpillar makes an arc shape. When one side of the caterpillar is returned to its original state, the friction with the surface pushes the silicon caterpillar forward.

Other pneumatic actuation systems have been reviewed in the literature. A paper by Tang et al. [28] highlights programmable active kirigami metasheets and analyses the use of origami metamaterials and different forms of actuating them. One form uses four pneumatic actuators to simulate the movement of a spider. Although the spider origami actuation method cannot be applied for morphing expanding gears since it relies on fast bursts of pressurised air, the caterpillar concept could be a viable option for expanding gears. Silicon blocks could be placed inside the gear, and when the gear needs to expand, the air is pumped into the silicon cavities, increasing the pressure and expanding the gear. Unfortunately, this actuation system would face two major challenges. Firstly, maintaining high pressure without leakages during a long period can be a challenging task. And secondly, the silicon can only be compressed by 55% of its original volume. Other alternatives, such as the Hoberman ring, can be theoretically compressed by a factor of 12 [28]. This leads us away from choosing pneumatic actuation systems as their potential expansion ratios would be limited compared

to alternatives, which would limit the gearing system's achievable gear ratios significantly.

2.4.3 Thermal

Thermal actuation is very common in the literature. Unfortunately, using varying temperature gradients to morph metamaterials is mainly used in origami, where the metamaterial does not have to overcome high loads. Therefore, most of the time, it is used in low-load applications. While this may work in a small-scale prototype, its lack of potential to scale up to a larger gearing system where belt tension produces large loads is what ultimately makes it unsuitable for the shape morphing CVT.

2.4.4 Motorised

Servo motors are one of the most common methods of actuation. This is due to their simplicity, ease-of-control and affordable price. The paper by Ryan L. Truby [29] proves the feasibility of this approach by using HS-5585MH servos in soft robotics. A servo is used to turn a specific angle in order to actuate a robotic finger. As the servo angle increments in 15 degree steps, the finger bends. The servo is able to rotate 180 degrees, where the finger becomes fully bent.

A paper by Brandenbourger M. [30] evidences how accurate control can be maintained using a motor. Brandenbourger explains how the torque resolution of a DC motor can be as low as 0.008mNm while the response of the motor to an input is 100Hz. Although, it is important to note that this delay arises from the controller, an Arduino ATmega32U4.

Overall, the literature reassures the idea that a servo motor actuation based system is a good method of control for shape morphing CVT gears within our constraints. It fits our requirements of high resolution for continuous gear ratios, fast response, and, importantly, affordability due to our limited budget of £75.

Chapter 3

Design Philosophy

Design philosophy in the context of this project is defined as the theoretical and practical considerations that determine the overarching approach applied to the entire project and all relevant sections of design and development. This approach allows for a universal set of goals and requirements to drive the decision-making throughout the entire iterative design process and allows for a consistent structure that is evident in the reasoning applied and compromises made throughout the design process. To summarize: the design philosophy of this project was to achieve the following:

1. Consider and implement all aspects of the project proposal.
2. Cohesively integrate existing literature into theoretical calculations, design concepts, and methods.
3. Construct a functional prototype of the major elements. Where intellectual contribution and advancement of existing designs are evident.
4. Create a clear, direct, and cohesive thesis which reflects the requirements and method of the project.
5. Clearly indicate future improvements in the theoretical and practical aspects of the project

Decisions made throughout the project reflect the design philosophy, and the reasoning which determined the summary is expanded on below.

3.1 Metamaterial Applications in CVTs

Traditional pulley-based CVTs function using two sets of inversely actuated cones and a transmission belt which sits between the cones, as seen in **Figure 3.1**. As the distance between the two cones that make up the input gear increases, the diameter of the input gear decreases. The diameter of the output gear is then reduced by inversely actuating the output gear cones to move closer together. This mechanism allows for seamless gear changes and, when utilized in snowmobiles and small vehicles, it can avoid torque drops.

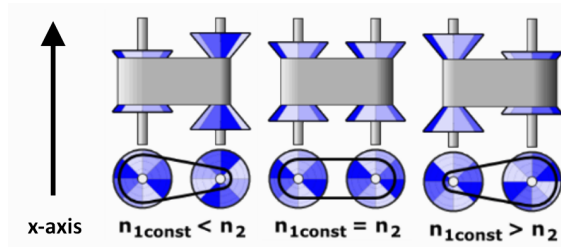


Figure 3.1: Traditional pulley-based CVT

Considering that the shafts of the CVT lay along the x-axis, the space that the device takes up along this axis will constantly increase and decrease depending on the gear ratio requirement. Referring to **Figure 3.1**, the minimum space that the CVT will consume in the x-axis will be the distance between the bases of the two cones when $n_{1const} = n_2$. The maximum space it will consume in the x-axis will be the distance between the bases of the two cones when n_{1const} is at a maximum or when n_2 is at a maximum. The space consumed along the y and z-axis will be the same due to circular nature of the input and output gears and it will always be the size of the diameter of the base of the cones. From this, we can conclude that traditional CVT mechanisms can be bulky and require a lot of space to operate.

The goal of this thesis is to develop an alternative CVT system, discarding the traditional large and bulky cone base and replacing it with a material or structure that is able to increase and decrease in diameter (an essential requirement for a CVT) while remaining constant size in the x-axis. This would allow for a very narrow CVT design that performs the same role as a pulley-based CVT while saving significant space. This requirement led to the investigation of meta-structures in gearing systems.

Metamaterials and meta-structures are structures and materials that are developed to react to forces in an unnatural way and have a response to forces that would not be found in traditional, solid materials. This unnatural response to forces can be achieved by creating a metamaterial (or meta-structure) out of multiple parts or by adapting materials to fold and pack in unique ways. Due to their irregular response to forces, metamaterials are an excellent solution to use in space saving applications and areas that require momentary size increases. We believe that CVT gearing systems can be designed that consume less Euclidean space than traditional CVTs and that using metamaterials is the key to this design problem. By using a meta-structure, a gear can be designed such that it expands and contracts as required while remaining narrow in the x-axis at all times.

Applying the knowledge gained from research on metamaterials and meta-structures, we have developed two designs that can be implemented in the place of traditional CVTs that will result in a reduction in Euclidean space, specifically along the x-axis.

The first alternative explored was an expanding pulley mechanism. It consists of three elements – nine pins that create the surface for the belt to sit on, a lower arm that contains the pins and allows them to move inwards and outwards, thus creating an expanding gear and an upper arm that holds the pins in place and guides them as they move inwards and

outwards. The elements and setup can be seen in **Figure 4.9**.

The expanding pulley mechanism remains constant size along each axis for all gear ratios while being narrower than a traditional CVT along the x-axis. The y-axis and the z-axis size is dependent on the maximum radius of the upper and lower arm of the expanding pulley. Since the expansion of the gear is not dependent on the x-axis, the radius of the pulley can be increased significantly while still maintaining the narrow size in the x-axis. This will be a favorable characteristic for the expanding pulley at larger sizes.

The second alternative to traditional CVTs is the Hoberman mechanism elaborated upon in **Section 2.3**. The mechanism comprises of several scissor patterns connected by pins or small shafts and the scissor-like parts are able to rotate around the pins. By creating a large, circular mechanism using the scissor-like structures, we are able to produce a gear that can expand and contract when actuated. It has been designed so that all of the central pins provide a surface for the belt to sit on. This mechanism can be seen in **Figure 4.29a**. The Hoberman mechanism can be designed to be as narrow as required which allows the goal of space saving in the x-axis to be achieved. Along the y and z-axis, the device will be at maximum size when the gear is at a maximum size, but as seen in **Figure 4.29a** the outermost pins move closer to the centre of the Hoberman when the gear contracts, thus creating momentary space saving during contraction.

Both the expanding pulley and the Hoberman mechanism have the potential to prove the hypothesis to be true by demonstrating Euclidean space saving along the x-axis. The momentary decreased of the Hoberman ring in space consumed in the y-plane and z-plane may seem minuscule and insignificant at the scale that the model has been manufactured, but consider that the device will be scaled up and used in larger applications and at a larger scale the amount of space saved will increase significantly. Moreover, using arms to push the Hoberman radially outwards, means that it cannot maximise this advantage. Since the Hoberman cannot contract fully due to the arms, the outer radius does not decrease significantly. This occurs because the contraction of the outer radius is most significant at full contraction.

3.2 Comparison Methods

In order to carry out a valid comparative analysis, a frame of reference needs to be established. As a result, we decided to investigate and compare the two possible solutions to reduce space in the axial direction. The three mechanisms that will be compared are:

1. *Conventional CVT*
2. *Hoberman*
3. *Expanding Pulley*

In order to test and compare the expansion ratio, we will employ a simple technique of expanding and contracting the device over a sheet of grid paper. This will allow us to very clearly observe whether the device is smaller in the y and z-axis when contracted than when

expanded. Another method that could be used to test the same aspect would be to create a square frame that has a side length that is equal to the diameter of the fully expanded Hoberman mechanism and place the device inside the frame. When contracting it, we will be able to observe whether there is a reduction in space consumption. These two simple methods will also allow us to determine the expansion ratio of each system.

To measure the thickness of each assembled prototype mechanism we used a caliper. We will use **Eq. 6.3** to calculate the theoretical width of an equivalent radius and gear ratio traditional CVT and compare.

3.3 Project Limitations

As the design progressed in its development it became clear that the limiting factor to the complexity of the design would not be limited theoretical understanding or calculations, but the following factors: Budget, equipment, manufacturing capabilities, design constraints, and time.

3.3.1 Budget

Any engineering project with a defined budget faces decisions during product development on where to compromise in terms of quality and quantity. Material costs significantly limit a design as the price increases with the design's size, complexity, and quality. Compromises must be made, and designs need to be adapted. The budget of this project was set at £75. Refer to BOM in **Table F.1** in **Appendix F**

3.3.2 Equipment

Available equipment is another significant contributor to the design philosophy followed throughout product development. The University of Edinburgh Mechanical Teaching Lab G.20 is a well-equipped space with industrial tools such as drills, a laser cutting machine, and 3D-printers, and was available for our use over multiple weeks.

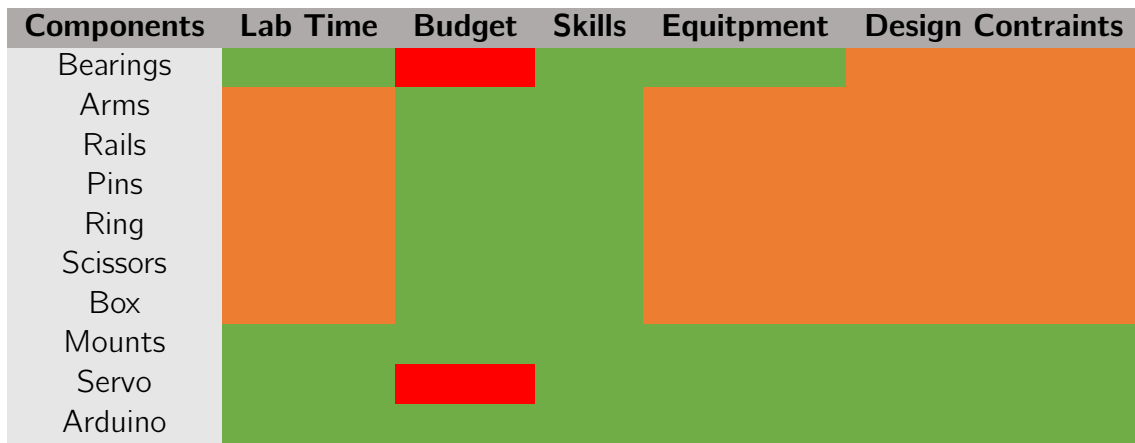


Table 3.1: Limitations that influenced each task
 Red - Major Limitation, Orange - Minor Limitation, Green - Negligible limitation

As seen in **Table 3.1**, limiting factors relevant to building the design need to be considered as a significant component of our design philosophy. However, not all these factors are obvious when the project begins, thus, adaptation is critical when circumstances change, such as when the Lathe machine became unusable as the shaft thickness were determined to be too small to make use of the machine.

3.3.3 Skills

In an engineering project, each member of a team or group adds a unique set of skills to the toolbox. Efficiency requires compromise and commitment, thus finding each member's strengths was a focus throughout the project. However, a complex and theoretical project such as this also required members to learn new skills with little time.

3.3.4 Design Constraints

A significant driving factor of the project was to create a CVT solution that fills less space than a traditional CVT, which limits the design to a compact form factor from the beginning. The only physical design constraint set was to minimize the axial shaft space of the CVT system while having a prototype to present in a classroom.

3.3.5 Time

Understanding the significance of the physical time limitations to manufacture and test was integral to the design philosophy. For example, the University of Edinburgh G.20 lab was only available to us on Mondays and Fridays from 9:00 am-12:00 pm for 4-5 consecutive weeks, limiting the time in which the prototype design could be constructed and tested.

3.4 Risks and Mitigation

Risk	Mitigation
Time and resource constraints will make the plan unfeasible.	During the analysis phase perform an in-depth feasibility study to assess the plan's viability. If the assessment indicates the plan is not feasible, return to the planning phase. Repeat this mitigation process until the feasibility study has a positive outcome
Manufacture may be too complex and time-consuming.	Perform small-scale, mock manufacturing to assess the time and complexity. If it proves too time-consuming, return to the design phase. Repeat this mitigation process until an achievable manufacturing plan is reached.
The design does not meet the required need.	Utilize an iterative design process, allowing time for multiple versions of each part. Continue iterating until the design meets the need.

Table 3.2: Risks and mitigation

Chapter 4

Materials and Methods

4.1 Theory of Hoberman Ring

4.1.1 Scissor Pattern Derivation

The Hoberman mechanism is a complex system that requires extensive geometrical calculations to ensure the maximisation of its geometrical characteristics. When analysing the Hoberman mechanism we will be considering its geometrical properties at 2 different points: collapsed state and expanded state. From the definition of expansion ratio seen in **Eq. 4.1**, we can tell that the expansion ratio is dependent on the collapsed & expanded inner radius.

$$\Delta A_{inner} = \frac{A_{Expanded}}{A_{Collapsed}} = \frac{\pi \cdot r_{inner@expanded}^2}{\pi \cdot r_{inner@collapsed}^2} = \left[\frac{r_{inner@expanded}}{r_{inner@collapsed}} \right]^2 \quad (4.1)$$

The expanding ratio for the outer ring of the Hoberman can be seen in **Eq. 4.2**.

$$\Delta A_{Outer} = \frac{A_{Expanded}}{A_{Collapsed}} = \frac{\pi \cdot r_{max}^2}{\pi \cdot r_{min}^2} = \left[\frac{r_{max}}{r_{min}} \right]^2 \quad (4.2)$$

We will be using the diagram shown in **Figure 4.1** to calculate the minimum radius and the collapsed inner radius. In **Figure 4.1** we can see the hoberman ring fully collapse, where it has maximum angle alpha, α_{max} . We can also see that the inner circle is actually a polygon with the same number of sides as number of scissor patterns in the Hoberman ring.

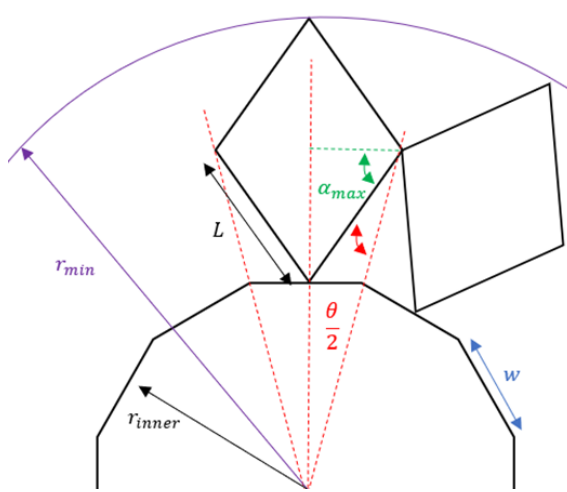


Figure 4.1: Hoberman geometry at collapsed state

Let us first find the equation for r_{min} . To find r_{min} we use simple trigonometry as seen in **Figure 4.1** to find the distance between $r_{min} - r_{inner@collapsed}$. Using trigonometry, we find **Eq. 4.3**, **Eq. 4.4** & **Eq. 4.5**:

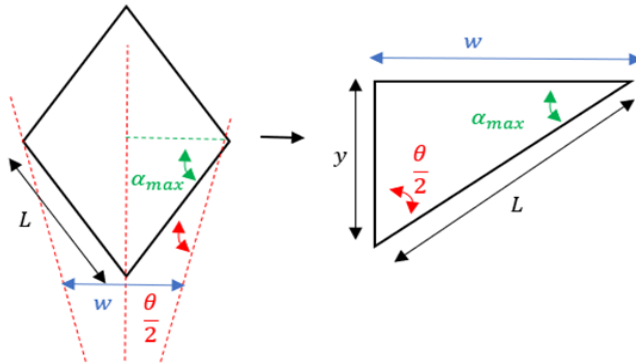


Figure 4.2: Trigonometric representation of Hoberman in collapsed state

$$r_{min} - r_{inner@collapsed} = 2 \cdot y \quad (4.3) \quad \sin\left(\frac{\theta}{2}\right) = \frac{w}{2 \cdot L} \quad (4.4) \quad \sin(\alpha_{max}) = \frac{y}{L} \quad (4.5)$$

We may now substitute **Eq. 4.5** into **Eq. 4.3** to find **Eq. 4.6**:

$$r_{min} = 2 \cdot L \cdot \sin(\alpha_{max}) + r_{inner@collapsed} \quad (4.6)$$

Now we are able to find the length of the inner collapsed radius $r_{inner@collapsed}$. We can use polygon angle theory **Figure 4.3** to find the angle α_{max} .

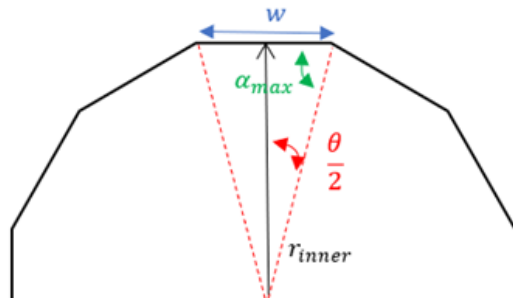


Figure 4.3: Polygon angle theory to find α_{max}

From **Figure 4.3** we can find the angle α_{max} , as seen in **Eq. 4.7**:

$$\alpha_{max} = \frac{(n-2) \cdot \pi}{2 \cdot n} = \frac{\pi}{2} - \frac{\pi}{n} \quad (4.7)$$

Furthermore, we can use trigonometry on the right angle triangle inside the polygon to find $r_{inner@collapsed}$, as seen in **Figure 4.4** and **Eq. 4.8**:

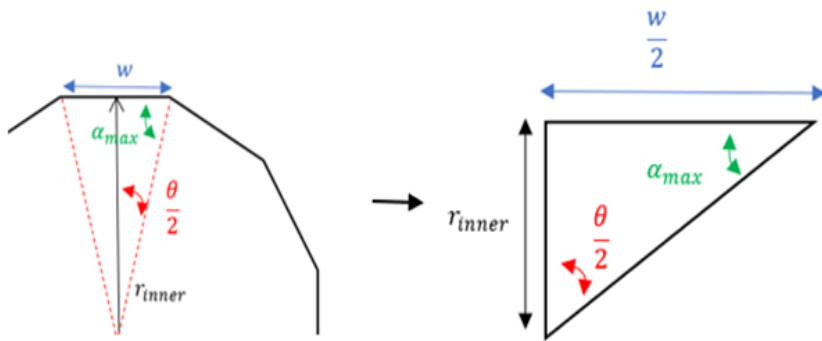


Figure 4.4: Using trigonometry to find r_{inner}

$$r_{inner@collapsed} = \frac{w}{2} \cdot \sin \alpha_{max} \quad (4.8)$$

If we now substitute **Eq. 4.7** into **Eq. 4.8** and rearrange to make $r_{inner@collapsed}$ the subject, we find **Eq. 4.9**:

$$r_{inner@collapsed} = \frac{w}{2} \cdot \sin \left[\frac{\pi}{2} - \frac{\pi}{n} \right] \quad (4.9)$$

We must now analyse the geometry at expanded state. This can be done using **Figure 4.5**.

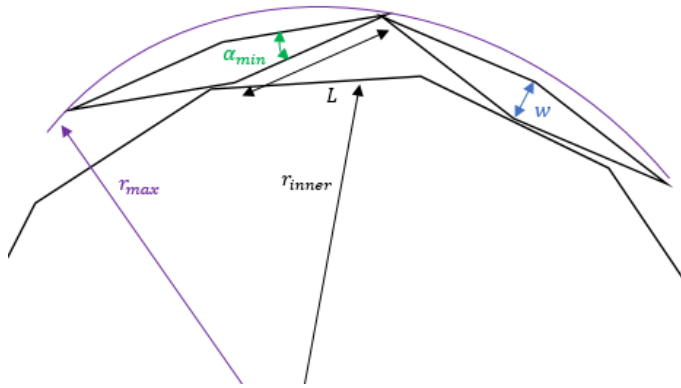


Figure 4.5: Hoberman geometry at expanded state

The distance between L in the inner radius and L in the outer radius is the width of L as in **Eq. 4.10**.

$$r_{inner@expanded} = r_{max} - w \quad (4.10)$$

We must also consider that the scissor patterns in the Hoberman will not be straight. To calculate the arc of L we will use **Eq. 4.11**

$$\theta = \frac{\pi}{n} \quad (4.11)$$

4.1.2 Expanding Arms Derivation

Now let us look at the arms that push the Hoberman to expand radially. The arms pushing the Hoberman can only be displaced by the diameter of the shaft holding the arms. Hence the arms have a maximum radial displacement of $2 \cdot r_{arm}$ (assuming the radius of the arms and the shaft are the same). **Figure 4.6** demonstrates how the arms would move causing the Hoberman to expand and that the maximum vertical displacement is the diameter of the expanding arc. **Eq. 4.12** is half $r_{inner@expanded}$ of the Hoberman, to ensure the Hoberman expands fully. The radius of the rotating shaft that holds the arc arms via pins must have the same radius as the arms to ensure full contraction of the arms at contracted state. **Figure 4.7** has been used as the reference length in deriving both **Eq. 4.12** & **Eq. 4.13**. Where **Eq. 4.13** makes reference to the arc length of the arm, which is half the circumference of the shaft. Moreover, the arm must have an arc shape, otherwise, in the case of a straight beam arm, it will overlap the shaft which would interfere with the servo rotating the shaft from the center. Having an arc which is half the circumference and same radius as the shaft means we are taking maximum advantage of its geometry. The arc can be tightly packed inside the shaft when the Hoberman is contracted. In addition, it takes full advantage of geometry in the expanded state, since it has the same radius as the shaft, hence a maximum expansion ratio of 4 in the arms.

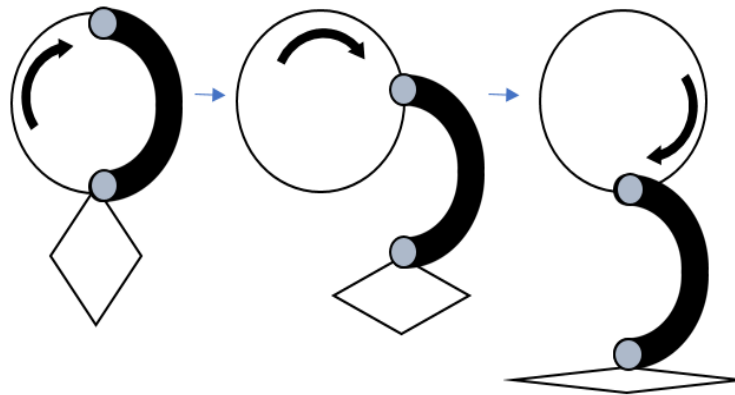


Figure 4.6: Expanding arm stages. Left: contracted Hoberman; center: mid-expansion of Hoberman; right: fully expanded Hoberman

$$r_{arm} = \frac{r_{inner@expanded}}{2} \quad (4.12)$$

$$C_{arm} = \pi \cdot r_{arm} \quad (4.13)$$

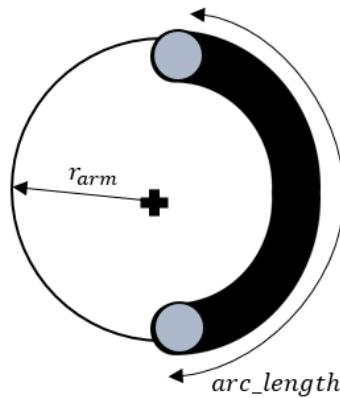


Figure 4.7: Expanding arm geometry

It is important to note that the Hoberman's contracted inner radius will be affected by r_{arm} . The Hoberman's $r_{inner@collapsed}$ will only contract to the radius of the arm, r_{arm} . Therefore, this will limit $r_{inner@collapsed} = r_{arm}$. Thus, a maximum expansion ratio of $\Delta A_{inner} = 4$ [22].

4.1.3 Limiting Factors and Assumptions of the Hoberman

Limiting Factors:

- The actuating arcs have an maximum $\Delta A_{inner} = 4$ [22].
- $\Delta A_{inner} \propto \frac{1}{r_{inner@collapsed}^2}$ from **Eq. 4.1**, and we know $r_{inner@collapsed}$ depends on w from **Eq. 4.9**. Thus, $r_{inner@collapsed} \propto w$. Therefore, the smaller the width, the smaller $r_{inner@collapsed}$ and the greater ΔA_{inner} . Hence, we aim to have the lowest **width**.
- From **Figure 4.8**, experimental results of parametric optimization of the scissor mechanisms accounting for physical dimensions were used to choose the number of sides, **n**, according to ΔA_{outer} . From this we find the limitation to be a point at which increasing the number of scissor patterns in the polygon does not increase ΔA_{outer} .

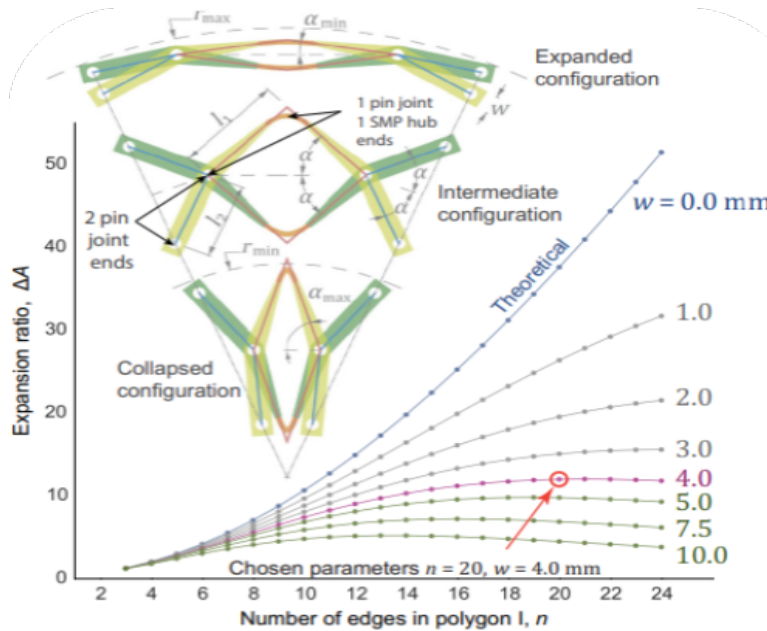


Figure 4.8: Parametric optimization of the scissor mechanisms accounting for physical dimensions [1]

Assumptions:

- When the Hoberman is in the expanded state, as seen in **Figure 4.5**, $\alpha_{min} \neq 0$. In theoretical calculations, we have assumed $\alpha_{min} = 0$. Therefore, when assembling the Hoberman in SolidWorks, we will expect to have a slightly smaller value of L.
- We assume L is a straight line when we go through theoretical calculations, while in reality it will have a slight angle to form an arc (**Eq. 4.11**). This will not affect expansion ratio, but will affect the shape of the Hoberman ring.
- We will not consider the actuation arc arms' stress limitations yet. We will only consider extracting the maximum expansion ratio from the Hoberman ring.
- We assumed $\alpha_{min} = 0$ when deriving **Eq. 4.10**. Hence, when expanding the Hoberman ring, the limitation between the inner and maximum radius is the width.

4.2 Iterative Design of the Hoberman

In our first iteration to maximise the expansion ratio, we had to minimise width. To ensure frictionless spin between the pin joints, we would use a bearing. We found a bearing of 3mm diameter that would fulfill our limitations seen in **Section 3.3**. Thus, $w > 3\text{mm}$. We would need a slightly larger width to hold the bearing within the structure. Hence, we chose $w = 5\text{mm}$. If we now look at the line $w = 5\text{mm}$ in **Figure 4.8**, we can tell that the maximum expansion ratio is at $\Delta A_{Outer} = 10$ (when the curve flattens) and this is at $n = 18$. From simulation seen in **Figure 4.21**, we found that the scissor patterns would not be able to withstand the belt tension. Although the first iteration design has an extremely large ΔA_{Inner} , this would be wasted by the fact that ΔA_{Inner} can only be a maximum of 4, as delimited by the arms. Hence, the focus changed in the following iteration to having $\Delta A_{Inner} = 4$ and a width that can withstand the belt tension.

In the second iteration, the width was increased to 10mm as it would withstand the tension of the belt. In addition, the number of scissor patterns can be decreased as the maximum expansion ratio now occurs at around $n = 12$. Hence, $\Delta A_{Outer} = 5$. Although, this will be close to the most optimal design from the geometrical point of view, it requires at least 6 arms to ensure the belt does not contract the Hoberman scissor patterns that are not held by the arms, hence deforming the circular shapes. Additionally, the greater the number of arms, the greater the length of the Hoberman in the axial direction.

For the final iteration we decide that 4 arms and 8 scissor patterns is the optimal design. In this way, for every two scissor pattern an arm will be connected improving the structural rigidity of the Hoberman mechanism. Therefore, $\Delta A_{Outer} = 1.8$ as n has been decreased. Although ΔA_{Outer} can be greater than 1.8, as seen in **Figure 4.8**, this would mean a smaller L . From simulation, we found that a 6mm pin would be enough to maintain the structural rigidity. Hence, in order to fit the pin inside length L , $L > 12\text{mm}$. Therefore, L was increased to 24.7mm since 2 pins are attached at each end of the scissor. This meant a $\Delta A_{Outer} = 1.8$. From the equations derived in **Section 4.1**, the dimensions are obtained. The dimensions are shown in **Table 4.1**. Step-by-step calculations can be found in **Appendix B**.

Component Name	Unit	Iteration 1	Iteration 2	Iteration 3
n	-	18	12	8
w	mm	5	10	10
ΔA_{Inner}	-	545	4	4
ΔA_{Outer}	-	10	5	1.8
r_{max}	mm	67.5	67.5	67.5
r_{min}	mm	21.3	30.2	50.3
$r_{inner@collapsed}$	mm	2.5	4.8	4.6
$r_{inner@expanded}$	mm	62.5	57.5	57.5
α_{max}	radians	1.4	1.31	1.2
L	mm	9.6	13.1	24.7
r_{arm}	mm	-	28.75	28.75

Table 4.1: Dimensional iterations of the Hoberman

4.3 Theory of Expanding Pulley

An alternative option to the conventional CVT system is to implement an expanding pulley mechanism as the CVT itself. Similar to the Hoberman mechanism, the expanding pulley will work by expanding the belt to the required size. The expanding pulley is commonly used to change the gearing on a machine by changing the gear ratio efficiently ensuring a smooth transmission.

In our design, the expanding pulley will consist of three parts: the upper arm, the lower arm, and the pins as seen in **Figure 4.9**.

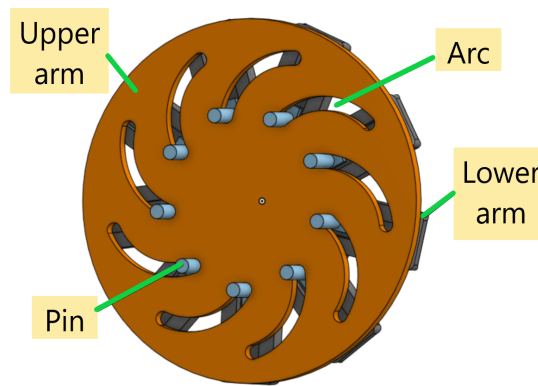


Figure 4.9: Draft design of expanding pulley in contracted form

As animated in OnShape (**Appendix A - S6**), the belt will be placed along the pins which will be pushed inwards and pull outwards by means of the curved arcs, increasing and decreasing the size of the belt when the upper arm is spinning. From the definition of expansion ratio in **Eq. 4.14**, the maximum expanded radius and minimum contracted radius of the expanding pulley determines the expansion ratio.

$$\Delta A = \frac{A_{Expanded}}{A_{Contracted}} = \frac{\pi \cdot r_{maximum@expanded}^2}{\pi \cdot r_{minimum@contracted}^2} = \left[\frac{r_{maximum@expanded}}{r_{minimum@contracted}} \right]^2 \quad (4.14)$$

The maximum expanded radius and minimum contracted radius of the expanding pulley are taken from the center to the position of respective pins as shown in **Figure 4.10**. A MG996R servo will be used in our design which acts as a motor to expand the pulley. The servo will be connected to the lower arm which needs to stay fixed, whereas the upper arm will spin. When the upper arm spins, the pins will start to expand alongside the belt. To begin the iterative process of establishing a workable expanding pulley structure, limiting factors are identified and assumptions are made.

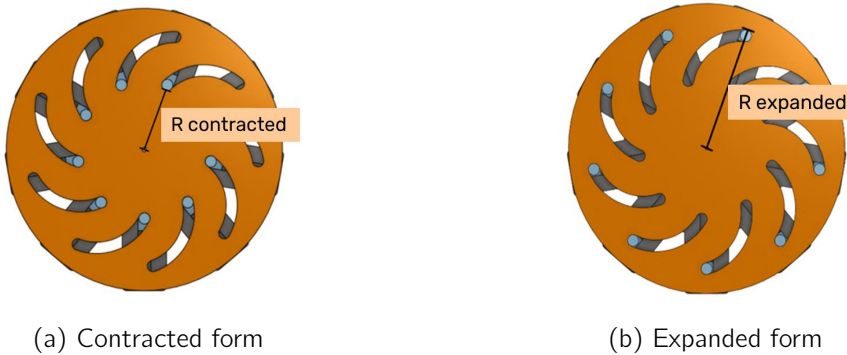


Figure 4.10: The two states of the expanding pulley

4.3.1 Limiting Factors and Assumptions of the Expanding Pulley

Limiting Factors:

- The size of the shaft limits the size of the contracted pulley. We aim to achieve the minimum possible size of pulley when contracted, to increase ΔA .
- The belt placed along the pins needs to form an approximately perfect circle. A larger number of arcs in the upper arm means a greater number of pins that can be slotted in. Thus, the closer the shape of the expanded pulley to a circle. However, the arcs cannot intercept with each other when designing the upper arm. Hence, an optimum number of arcs need to be chosen to ensure an almost perfect circle without the arcs intercepting one another.
- The lower arm needs to be fixed when the servo is rotating. Hence, we need to use a bearing to prevent the lower arm from spinning. This results in a smaller contraction radius. Hence, a decrease in ΔA .

Assumptions:

- The diameter of the expanding pulley is designed such that it has the same size as the Hoberman ring. This makes it easy to compare the two mechanisms.
- The usual design of an expanding pulley, as shown in **(Figure 4.11)**, has a pulley arm whereby the maximum expansion ratio that can be achieved by the design is $\Delta A = 2$. By having pins in our design instead of pulley arms and placing the belts on top of the pins, the maximum expansion ratio achieved can be greater than two.

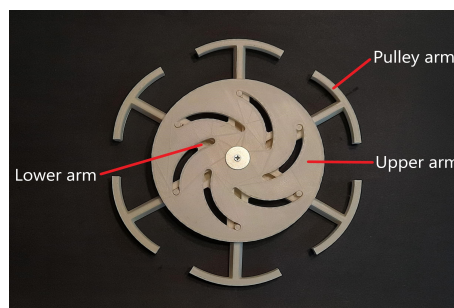


Figure 4.11: Conventional design of expanding pulley

4.4 Iterative Design of the Expanding Pulley

In our first iteration, the goal was to maximise the expansion ratio. To do this, the length of the arc needed to be maximised and brought closer to the center of the pulley so that the radius was minimised when the pulley was contracted. The contracted radius of the pulley needed to be smaller than the expanded radius to ensure a maximised ΔA as seen in [Eq. 4.14](#). In the first sketch of the upper arm [Figure 4.12](#), the diameter of the pulley is set to be 200mm and width of arc is 6mm. Nine is the maximum number of arcs that can be fitted without intercepting. However, the limiting factors are not yet fully considered in iteration 1. From this, we decided to use nine arcs in the future iterations of our design.

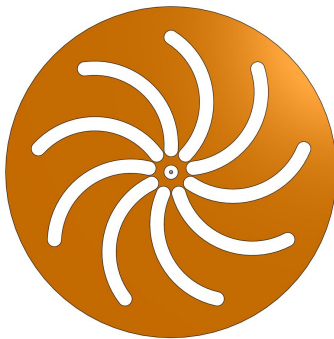


Figure 4.12: Draft design of expanding pulley in contracted form

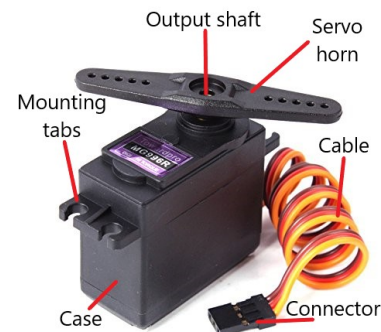


Figure 4.13: Labelled parts of the MG996R servo

The second iteration focused on coupling the servo ([Figure 4.13](#)) to the expanding pulley. The first idea was to make a cutout on the lower arm to fit the servo ([Figure 4.14](#)). The servo horn would then be attached to the upper arm by extruding a horn cut-out on the center of the upper arm's base. From this, when the output shaft of the servo spins, the horn will spin alongside the upper arm ([Figure 4.15](#)). Ideally, the case will stay fixed with the lower arm.

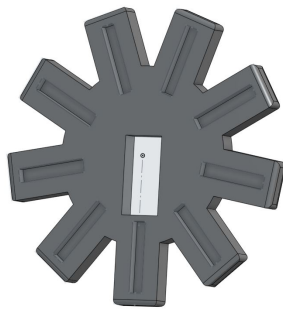


Figure 4.14: Cutout of servo in the center of the lower arm



Figure 4.15: Cutout of the servo horn on the base of the upper arm

However, when this idea was implemented in the design, we noticed that the size of the servo cutout on the lower arm would restrict the radius of the contracted pulley to be at its

minimum. As a result, the expansion ratio was smaller than expected.

In the third iteration, an approach was taken to couple the servo to the pulley without restricting the minimum contracted radius by using a servo-shaft coupler (**Figure 4.16**). The coupler would connect the servo's output shaft to the lower arm. The coupler was to be fitted to the output shaft of the servo and the other end would be attached to a 6mm diameter shaft (**Figure 4.17**).



Figure 4.16: The servo-shaft coupler designed in OnShape

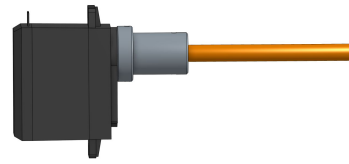


Figure 4.17: Servo-shaft coupler is used to connect the servo (left) and the shaft (right)

To ensure that the lower arm stays fixed and only the upper arm spins, a hole is made in the lower arm to fit the bearing in **Figure 4.18**. The bearing will hold the lower arm still as the 6mm diameter shaft is spinning.

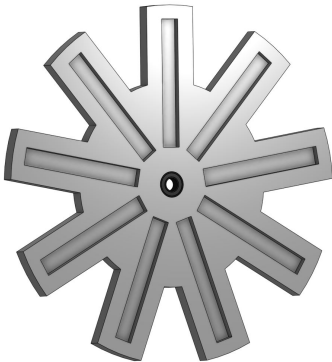


Figure 4.18: Bearing is fitted in the center hole of the lower arm

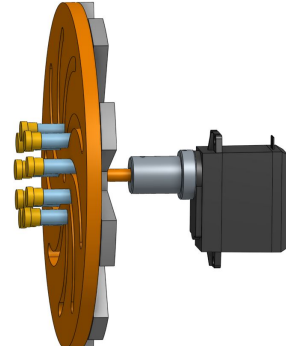


Figure 4.19: Side view of the final design

With this approach, the pins could be pushed inwards towards the center hole without having the size of the servo restrict it. Thus, producing a much smaller radius when contracted. As a result, this approach would maximize the expansion ratio.

For our final iteration, the diameter of the upper arm was set to be 140mm. This was so that there would be a 10mm space between the arc and the edge. The radius of the maximum expanded pulley was set to be 120mm. This value was taken to be approximately equal to the radius of the inner expanded Hoberman design to obtain a side-by-side comparison which would be further explored in **Section 6.2**. The final design obtained from the above iterative process, having an $\Delta A = 8.6$, is shown in **Figure 4.19**.

The expansion ratio and dimensions calculated from using equations discussed in **Section 4.3** are tabulated in **Table 4.2**. Step-by-step calculations can be found in **Appendix C**.

Component Name	Unit	Iteration 1	Iteration 2	Iteration 4
Width of arc	mm	6.0	6.0	6.0
$r_{maximum@expanded}$	mm	60.0	60.0	60.0
$r_{minimum@contracted}$	mm	14.9	42.6	20.5
ΔA	-	16.2	2.0	8.6

Table 4.2: Dimensional iterations of the expanding pulley

4.5 Simulations

4.5.1 Purpose and Theory

Simulations are a fundamental part of any iterative design process. Engineering simulations are done to confirm the performance of a part based on the 3D CAD model and the expected loads the components will experience when the assembly is functioning.

The simulations for the two proposals were done using SolidWorks Simulations. The following FEA simulation types were considered: Von Miches and Tresca. Von Miches is a critical distortion energy theory that produces a less complex output than Tresca. Von Miches was chosen as it does not apply a conservative overestimation of forces, as that was already accounted for in force estimation.

4.5.2 Types

Types of simulations completed on relevant parts

1. Static load of each individual part: load is slowly applied over time
2. Buckling: bifurcated load to find critical buckling
3. Non-linear loading: static loading at an angle
4. Linear dynamic load: constantly changing loads
5. Drop testing of full assembly

4.5.3 Method and Scissor Arms as an Example

The main goal of the loading / dynamic / motion simulations was to find the yield strength and failure condition of each part. Additionally, finding the critical failure point where any single part will fail and the operation of the Hoberman Mechanism will cease was paramount.

When failure or critical failure was reached, the part would undergo static and dynamic optimization. Resulting in the component dimensions having to change between iterations. Each part underwent the process shown in **Figure 4.20** to decide validity and requirement to perfect the design (the process for the scissor arms is used here as an example).

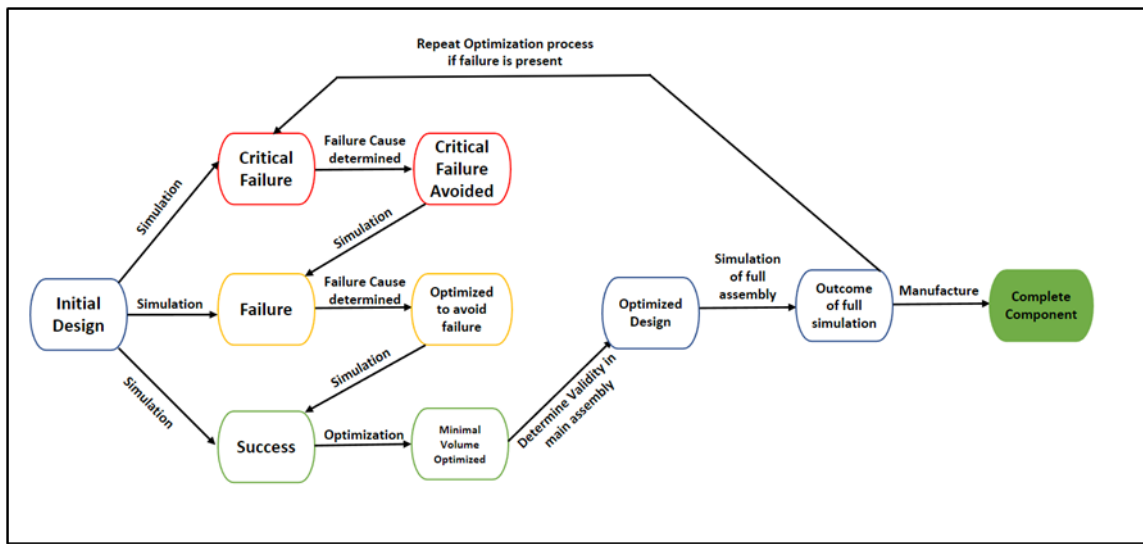


Figure 4.20: Diagram showing the optimization process for each part

SOLIDWORKS optimization works to minimize volume and mass, thus, minimizing material requirements and manufacturing time while supporting a geometry that allows the part to withstand the required loads. This often results in larger geometries as the loads are considerable and PLA is not a particularly sturdy material. The design is adapted based off of preset constraints and variables manually set for each part as shown in **Table 4.3**.

Variables	Parameters			
	Range of steps	Minimum value (mm)	Maximum value (mm)	Step
Width		5	15	0.1
Thickness		2.5	7.5	0.1
Constraints				
	Type	Minimum value (mm)	Maximum value (mm)	Step
Dimension 1	Pin hole	5	15	0.1
Dimension 2	Length	2.5	7.5	0.1
Goals				
	Aim	Requirement		
Volume	Minimize	Yield: no		
Mass	Minimize	Yield: no		

Table 4.3: Diagram showing the optimization parameters for scissor arms

The first iteration is simulated with each relevant simulation type. If a failure occurs, shown in **Figure 4.21**, the part is perfected using SolidWorks Simulation Optimization, i.e., the part geometry is changed within the predefined constraints. Expansion arm failure is shown in **Figure 4.22** below.

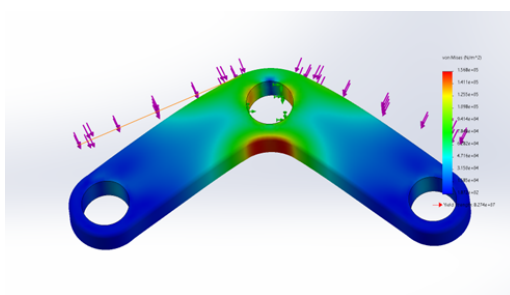


Figure 4.21: Diagram showing the failure of the scissor arm

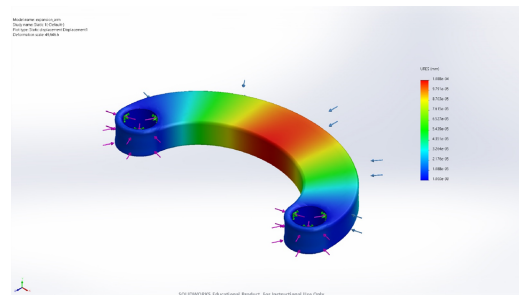


Figure 4.22: Diagram showing the failure of the expansion arm

The outcome of the scissor arm simulation process and optimization iterations are shown in the table below, where the complete table for all components can be found in **Appendix A**.

Component:	Scissor arm							Legend	
Type of Simulation:	Static	Dynamic	Fatigue	Buckling	Non-Linear	Linear Dynamic		Pass	
Applied								Fail	
Iteration Number	Critical Failure	Critical Failure Avoided	Failure	Optimized to avoid failure	Success	Min. Volume Optimized	Optimized Design	Outcome of full assembly simulation	Complete Component
1									
2									
3									
4									
5									

Table 4.4: Table showing the simulation outcome of optimization for the scissor arm

4.6 Manufacturing

4.6.1 Hoberman Ring

The manufacturing process for the Hoberman ring structure started with us determining the geometry of the scissor patterns by validating it with theoretical calculations and then inputting the dimensions into SolidWorks models which confirmed that the geometry can be assembled as intended, with 8 scissor arms. It is worth mentioning that the arms are bent by $360^\circ/8 = 22.5^\circ$ to allow the formation of the circular shape. In order to connect the scissor arms, endcaps were friction fitted onto 20mm long steel shaft pins which connected the scissor arms together, allowing for one degree of freedom (see **Figure 4.23a**).

Once the design was modelled fully, we 3D printed the scissor arms as shown in **Figure 4.23c**, using a Prusa Mini 3D printer with 0.4mm nozzle diameter and 1.75mm PLA filament. The tolerancing on the pin joint holes had to be redone multiple times to allow for the shafts to rotate with minimal friction. A vice was used to friction fit the endcaps onto the pins on both sides to hold the Hoberman ring together.

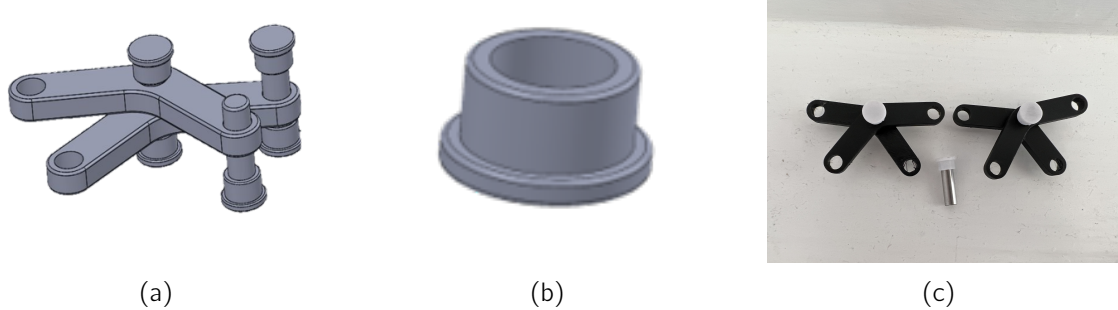


Figure 4.23: (a) Scissor pattern model (b) Endcap model (c) Manufactured scissor pattern



Figure 4.24: Loosely assembled Hoberman ring made of 8 scissor arm

The first laboratory session was spent cutting shaft into smaller pieces using a hacksaw. Due to the uneven surface finish left by the hacksaw, a sanding machine was used to smooth the tips and allow for easier insertion into the endcaps. Once all the caps were fitted, and the assembly of the Hoberman ring was finished (see **Figure 4.24**), the next step was to create a central core structure which would actuate the Hoberman ring.



(a) Central core (b) Expansion arm

Figure 4.25: Key Hoberman expansion mechanism parts

We connected two arms on the bottom and top of the central core to allow them to collapse inward without overlapping with each other. Each expansion arm pushes the

structure in one direction to allow a smooth expansion in each direction. The final assembled central core structure is shown in **Figure 4.26**.

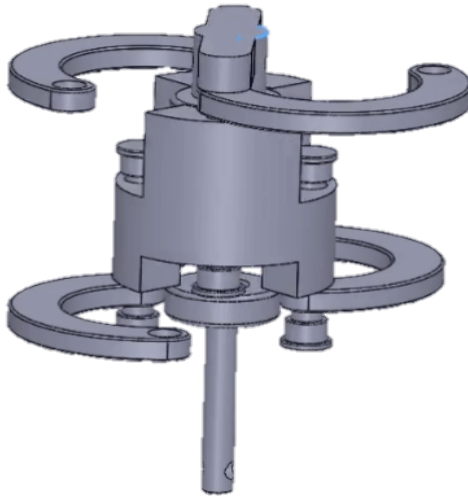
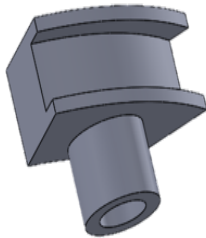


Figure 4.26: Central core with arms attached to it

To allow the rubber band (which was a placeholder demonstrator of a power transmission belt) to sit on the pins, a special rail structure was designed with walls on each side forming a channel to ensure the rubber band would not slide off the Hoberman ring (see **Figure 4.27b**).



(a) CAD model



(b) Manufactured prototype

Figure 4.27: Belt rail design

To attach the Hoberman CVT system, we made a cutout of plywood **Figure 4.28** to hold the structure in place while the two servos are attached from behind (**Figure 4.29b**). The two rails in the plywood are essential to prevent the Hoberman from rotating while it is being actuated by the shafts. This would collapse the actuation if it occurred and is discussed further in **Section 6.1.3**. Additionally, the holes on the plywood are there to hold the bearings (dimensions: $8 \times 22 \times 7 \text{ mm}$).

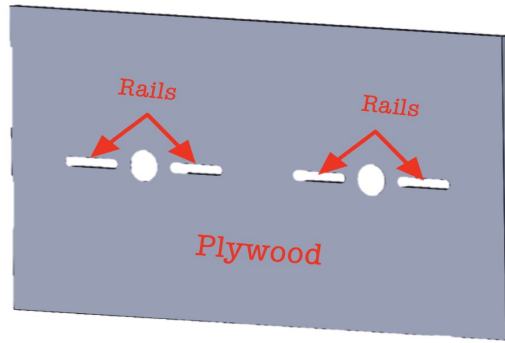
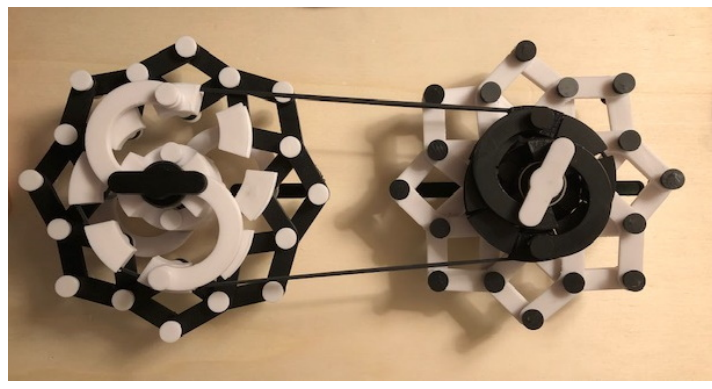


Figure 4.28: Plywood CAD model

The system was assembled and tested, shown in **Figure 4.29a**. A video of the prototype expanding can be found in **Appendix A.1**.



(a) Front face



(b) Back face

Figure 4.29: The final Hoberman CVT system assembly

4.6.2 Expanding Pulley

After going through the iterative design process described in **Section 4.3**, the final design with finalized dimensions was ready to be manufactured in the lab. Our design consists of three major parts as described in **Figure 4.9**. The upper arm and lower arm are manufactured by laser cutting plywood into their respective shapes. A plywood sheet with 6mm in thickness is used to laser cut the upper arm (**Figure 4.30a**). For the lower arm, we used two plywood sheets of 3mm thickness that were laser cut into their shapes and glued to each other using Evo-Stik Wood Adhesive (**Figure 4.30b**).

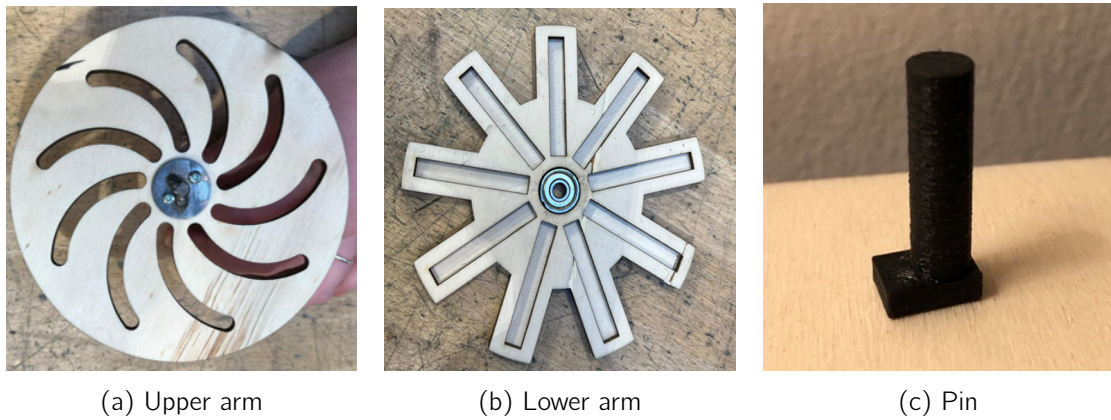


Figure 4.30: Manufactured expanding pulley parts in the lab

Once the glue had dried, we fitted a bearing with a 19mm outer diameter and inner diameter of 6mm through the center hole of the lower arm as can be seen in **Figure 4.30b**. This is done to ensure that when the shaft is rotating, only the upper arm is spinning and the lower arm stays fixed. On the top center of the upper arm, a steel disc of thickness 2.4mm with a hole of 6mm in its center was welded to the shaft which was placed through the hole of the upper arm as shown in **Figure 4.31**. The steel disc was then screwed to the upper arm.

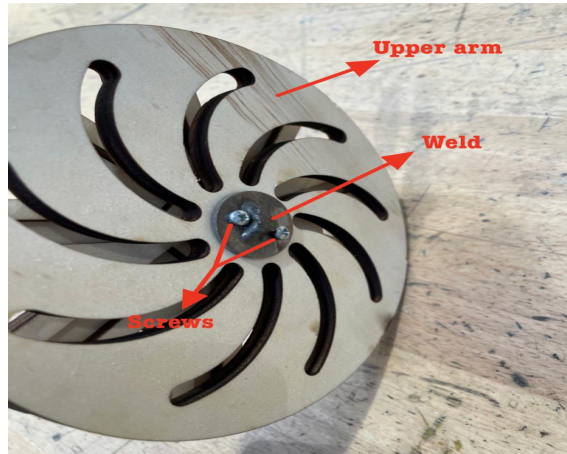


Figure 4.31: The upper arm, welded part, and screw positions

Next, the pins were manufactured via 3D-printing using the same material and 3D printer as used in manufacturing the Hoberman ring (**Figure 4.30c**). The pins were then placed in their respective channels on the lower arm, and, finally, the lower arm was ready to be connected to the same 6mm shaft.

4.6.3 Actuation

The inverse actuation was achieved by using the two MG996R servos mentioned previously. A potential divider circuit, as shown in **Figure E.2**, with two resistors R_1 and R_2 , was

used to control the voltage to the servos, where R_1 is fixed and R_2 is variable. The following equation $V_{out} = \left[\frac{R_2}{R_1+R_2} \right] \cdot V_{DC}$ was used to determine the output voltage. Refer to **Figure E.1** in **Appendix E** for the complete circuit diagram.

The servos angles are fixed between $[0, 180]$ such that, $\phi_1 = \in [0, 180]$ $\phi_2 = \in [0, 180]$. From this, we were able to map out the angle based on the voltage output as follows $V_{out} \in [0, V_{DC}]$, $\phi_1 \in [0, 180]$, $\phi_2 \in [180, 0]$. This meant that when the output voltage was at V_{DC} , ϕ_1 would be 180° , while ϕ_2 was zero. **Table 4.5** illustrates the mapping used in more detail.

Output Voltage	0	$\frac{V_{DC}}{2}$	V_{DC}
ϕ_1	0	90	180
ϕ_2	180	90	0

Table 4.5: Angle and voltage mapping used in the actuation system

From **Table 4.5**, one can notice three different primary scenarios:

- *Scenario 1*: when the output voltage is zero, ϕ_1 and ϕ_2 are 0 and 180 respectively, meaning that the gear ratios between both the expanding pulleys and both the Hoberman rings are 1:2.
- *Scenario 2*: when the output voltage is at $\frac{V_{DC}}{2}$, $\phi_1 = \phi_2 = 90$. This means that the gear ratio is 1:1.
- *Scenario 3*: when the output voltage is at its maximum value, $\phi_1 = 180$ and $\phi_2 = 0$, the opposite to scenario 1 occurs, which means there will be gear ratios of 2:1.

In addition to this potential divider circuit, another potential divider is used as a switch between two modes: wired and Bluetooth. Once an LED light in the circuit switches on, that indicates that the mechanism is now in the Bluetooth mode, connected with a HC-06 Bluetooth module to control the servos remotely. A control panel phone application called "Arduino BlueControl" (**Figure 4.32**) is used to pass actuation signals to the mechanism. The phone works as the transmitter and the Bluetooth module as a receiver.

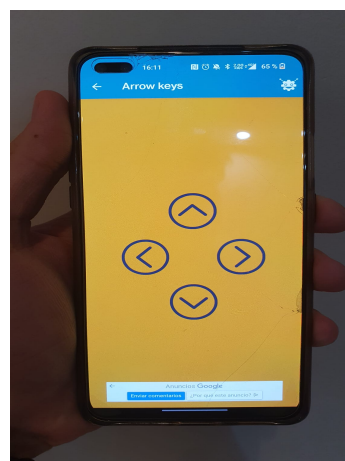


Figure 4.32: The Bluetooth application control panel

The right and left arrows, shown in **Figure 4.32**, result in a $+30^\circ$ degrees movement

and -30° respectively. Similarly, for the top arrow $+5^\circ$ and the bottom arrow -5° . Lastly, the actuation has a 15 *ms* response time from the input to the output. Further, the servo model we are using rotates at 60° per 0.2 seconds. Therefore, it will take the servo 215 *ms* to rotate 60° and 645 *ms* from 0° to 180° . The code for this part of the project can be found in **Appendix A - S3**.

4.7 Experiments and Modelling

We used a model to examine both the Hoberman and the expanding pulley in terms of measuring the amount of space it occupies when the structure is in the contracted or expanded position. For the Hoberman, the structure is relatively see-through, therefore we placed the structure on a grid as shown in **Figure 4.33**, where we measured the amount of expansion in terms of grid squares. The video recording of the contraction and expansion experiment is available in **Appendix A - S1 & S2**.

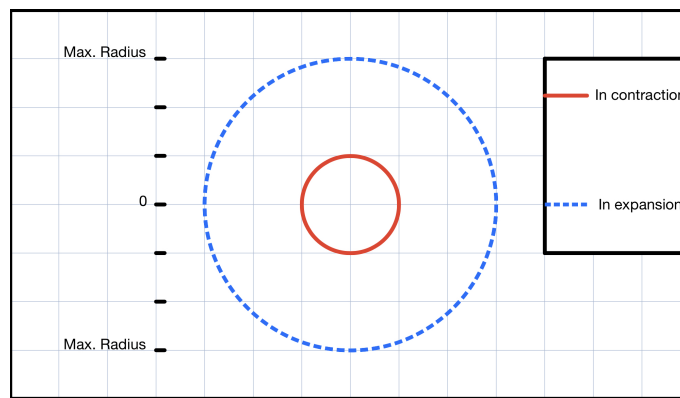


Figure 4.33: Hoberman expansion model

However, when doing the same thing with the expanding pulley, we would be measuring the movement of the pins relative to the center of the pulley as illustrated in **Figure 4.34**. To obtain the axial width of the Hoberman ring and the expanding pulley, we used a caliper on our small-scale prototypes.

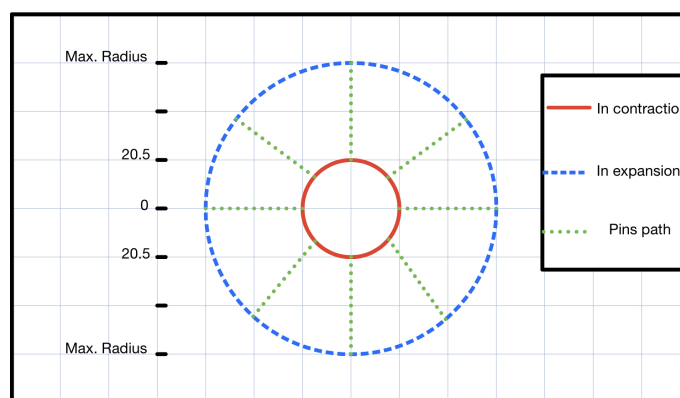


Figure 4.34: Expanding pulley expansion model

Chapter 5

Results

5.1 Analysis of Method

5.1.1 Theoretical Analysis

Hoberman

The Hoberman expansion ratio was limited by the geometry of the expanding arms from the center structure to the scissor arms. For the extension arms to endure the repeating expansion and contraction under load, the geometry of the individual component is made to be bigger than the ideal volume for that component to allow the maximum expansion ratio. Finding an alternative solution to the arc expansion arm would allow for a better expansion ratio by decreasing the minimum radius of the rails.

Expanding Pulley

The expanding pulley design was theoretically accurate, but neglecting friction rendered the method impractical in reality. This is evident in **Appendix A - S7** which shows that the small-scale expanding pulley prototype failed to actuate due to friction. This was due to the force applied by the upper arm on the pins being misaligned with the path that the pin can travel. The force acting in a different direction than the degree of freedom results in the pin being pushed into the side of the rail instead of being driven towards the center.

5.2 Width and Volume Reduction

The experiment and modelling were predominantly simulation based. The limiting factor to the connection between simulation and testing was that an optimized part frequently required a full rework of the expansion mechanism for the Hoberman.

As seen in **Appendix A - S1 & S2**, the small-scale Hoberman ring CVT prototype achieved successful expansion. The limitations of the assembly are also evident: the expanding arms clearly limit the minimum size by inhibiting further contraction due to the angle

at which they sit when contracted. The successful aspects can be seen in the fact that the device functions as planned: the scissor arms expand fully without bending and the fine tuned synchronous nature of the expansion and contraction of the two assemblies create a predictable gear ratio, which shows the validity of the Arduino code and the theoretical claim that the rotational actuation is transferable to any reasonable scale. The direct dimensions are reliant on the specific servo, but can be scaled with an appropriate motor that can provide enough torque for that relative scale.

5.2.1 Simulations

As mentioned before, the simulations were limited by the lack of a defined scale for the assembly. The simulations were, therefore, solely focused on geometric optimization. Linear and non-linear loading simulations for the Hoberman and expanding pulley led to resultant values in line with the theoretical calculations. This deemed the selection of both loading conditions and simulation method as valid. See **Table 5.1** for detailed results.

Hoberman		Scissor arm	Expanding arm	Central structure
Material	PLA	PLA	PLA	
Volume change	+17%	+14%	-5%	
Shafts		End caps		
Material	Stainless steel	PLA		
Volume change	-18%	-13%		
Expanding pulley	Ring	Pins	Rail structure	
Material	Plywood	PLA	PLA	
Volume change	-2%	-4%	0%	

Table 5.1: Results of simulations and geometric optimization

After the manufacturing process was completed and the theoretical and practical elements were compared, the qualitative results are summarized as:

Design	Results			
	Simulated	Manufactured	Saved space	Functioned
Hoberman	Fully	Fully - completely functional model	Yes	Yes
Pulley	Fully, but the theoretical friction co-efficient didn't match actual	Single pulley (1/2)	Yes	No

Table 5.2: Qualitative results of the manufacturing process

The simulations showed that components could be optimized to withstand forces relevant to that component, instead of a general application. This allowed for efficient material use within the Hoberman mechanism but increased the overall volume by **17%**. Volume reduction was a secondary goal, and the main goal of reducing axial space was achieved to a greater extent with the Hoberman reducing axial width by **15.5%**.

The total volume decreased due to the optimization reducing redundant material in areas not exposed to loading while maximizing strength at the weakest segments. Some components such as the central structure decreased by as much as **5%**, as the rotational motion and relevant loading of that component allowed for minimal material usage, whereas the scissor arms increased volume by **17%** due to the significant bending moment experienced by the component when expanding the Hoberman.

Belt slippage occurs when the torque applied to the belt overcomes the static friction between the belt and the rails. Rubber on rubber has a friction co-efficient of 1.35, but rubber on a metallic material is much lower.

Constructing the Hoberman proved that the expansion ratio was limited by the size of the expansion arms as was expected. The expansion ratio of the area could not exceed **1:4** as the expansion arms collided with each other when contracting. The scissor arms had to be long enough to expand to a useful diameter, but strong enough to not deform under actuation. Iterations **2** and **3** were designed with a minimal contraction diameter as the primary focus.

Iteration efforts led to the optimal design for the Hoberman being ΔA_{Outer} as seen in **Table 4.1**. This was found to be the optimal balance between expanding ratio, minimal geometric volume, and strength.

The same was applied to the expanding pulley with a maximum radius of 120mm and $\Delta A = 8.6$. Numerical results are available in **Table 4.2**.

Chapter 6

Discussion

6.1 Improvements in our design

6.1.1 Hoberman Pushing Arms

The current semicircular expanding arms are the best geometrical option, as they provide the maximum expansion ratio for the mechanism. Having said this, its geometry is a drawback when it comes to vertical deflection. This can be seen in equation **Eq. 6.1**. Since the arm is a half-circle, its arc angle is π or 180 degrees, hence maximum deflection. The full derivation of the vertical and horizontal deflection can be seen in **Appendix D**.

$$\delta_v = \frac{P \cdot R^3 \cdot \pi}{2 \cdot EI} \quad (6.1)$$

In addition, from simulation in **Figure 4.22**, there is a clear indication that the half-circle shape is indeed not the most structurally rigid shape. It will snap at 100N belt tension.

To avoid the structural instability there are different options for the geometry of the shape, for example, using straight arms. This would mean that the the expansion ratio would decrease due to the arms overlapping the center of the circle and they will be obstructed by the shaft as seen in **Figure 6.1**. This would result in a stiffer arm, but a reduction of the expansion ratio, which would be dependent on the thickness of the shaft. Furthermore, the vertical deflection of the straight arm would be 0mm, since the arc angle would be 0. Hence, much greater structural stability.

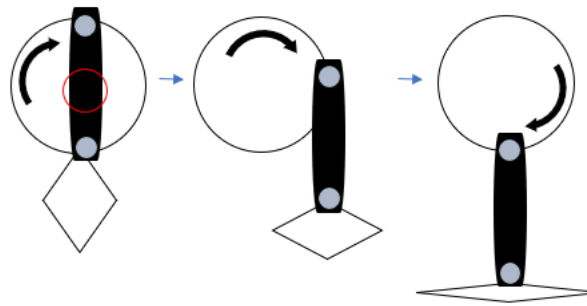


Figure 6.1: Straight expanding arms. Left image shows collision of the arms with the shaft at contracted state

Alternatively, we could ensure the loading in the arc is not directly vertical. Semicircular beams deflect vertically due to a vertical load. Hence, if we are able to change the angle of the load, we will be able to mitigate some of the deflection of the beam [31]. Finally, reinforcing the semicircular beam with rods in the vertical axis will prevent the beam from deflecting. In essence, this solution would be the combination of a straight beam that overlaps with a semicircular beam.

6.1.2 Increasing the Hoberman Outer Ring Expansion Ratio

The outer expansion ratio, ΔA_{Outer} can be increased. Increasing the outer ratio expansion is beneficial to have a greater momentary space reduction in the contracted state of the Hoberman ring [22]. In **Section 4.2**, ΔA_{Outer} has to be reduced to 1.8. This is necessary to be able to fit the pins in the scissor pattern, hence we have had to increase the length due to the diameter of the pins. If instead the design consists of lower diameter pins, we can decrease the length, L , of the scissor and increase the number of scissor patterns to increase ΔA_{Outer} . The improved version would have the potential of $\Delta A_{Outer} = 5$, with $n = 12$, and $L = 13mm$ [1]. This would require a pin with a diameter considerably smaller than 6mm.

6.1.3 Rotation and Actuation

One of the major flaws in the execution of the Hoberman CVT design is its inability to transmit power between an input and output shaft using a belt. This is because the state of actuation (expansion and contraction) of the Hoberman ring is derived from the rotation of the shaft at the center of the mechanism. The rotation of this central core pushes the expansion arms outward and rotates the Hoberman itself. The only reason the current design does not rotate is due to the rails in the plywood, which limit the motion of the Hoberman to be purely radial. The fundamental problem is the interference of the rotation and actuation of the Hoberman due to both processes occurring on the same axis. Any rotation of the central shaft causes actuation and vice versa.

The clearest solution to this flaw is to decouple the actuation and rotation of the mechanism. By looking closer at the Hoberman design, it can be seen that the expansion and

contraction is linear in the radial direction as discussed by Chen et al. [1], meaning if any single pin is followed while expanding, its path is straight (assuming the Hoberman itself does not rotate). Therefore, the Hoberman ring can in fact be actuated using a linear actuation mechanism in the radial direction of the ring. This means that there is an opportunity to decouple the actuation of the Hoberman from its rotation.

We propose a limited conceptual design modification to achieve this decoupling and allow for power transmission using the Hoberman CVT. **Figure 6.2** demonstrates roughly how this mechanism would function. A bell crank mechanism allows for the linear motion of a shaft to be transmitted to another perpendicular shaft. This means that the pushing of the central shaft can be transformed into a linear outward motion, pushing on the pins of the Hoberman and causing it to expand and contract. Similar solutions have been used in other connection composition and joint mechanisms such as those described by Parashar [32] and Byeong-Sam Kim [33].

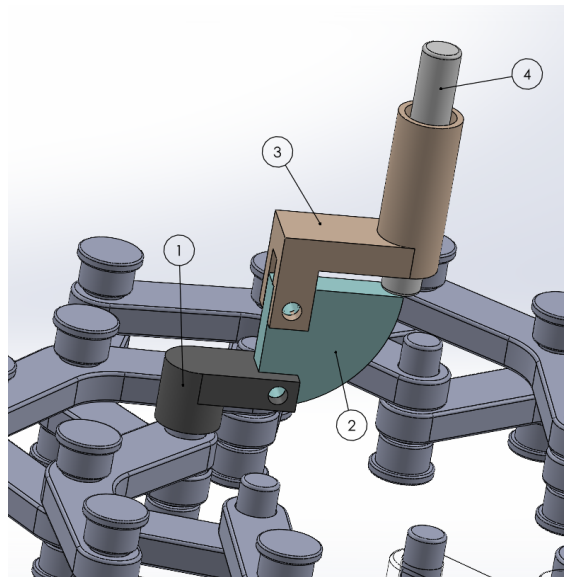


Figure 6.2: Potential mechanism allowing simultaneous actuation and rotation of the Hoberman ring

Figure 6.2 parts are labelled below:

1. Linear connector
2. Bell crank
3. Central connector
4. Central shaft

The central shaft would be mounted to a bearing and the central connector would go up to the bearing and be allowed to spin freely, however it would not move along the shaft axis. The shaft, on the other hand, would be connected to a linear actuator on one end allowing it to push on the end of the bell crank which would pivot around the central connector and

push on the linear connector, actuating the Hoberman ring through the inner pins. This conceptual idea would allow the Hoberman ring to rotate freely around the central shaft while actuating using the linear push / pull motion of the same shaft.

6.1.4 Expanding Pulley

When designing the expanding pulley in OnShape, as the upper arm spins, the pins will move along the arc of the upper arm. However, when assembling the expanding pulley after manufacturing the parts in the lab, we found that the upper arm failed to move the pins along the arc when being spun as mentioned in **Section 5.1.1**. When investigating why our design of the expanding pulley did not work, we concluded that this problem arose due to the material selection for manufacturing of the upper arm, lower arm, and the pins.

As mentioned in the manufacturing section, the upper and lower arm are made of plywood, meanwhile the pins were made of PLA. The friction coefficient of plywood is around 0.3 to 0.5 [34] and PLA is approximately 0.49 [35]. When the upper arm is spinning, the force applied by it to the pin is in a perpendicular direction which is the normal force, R , as seen in **Figure 6.3**.

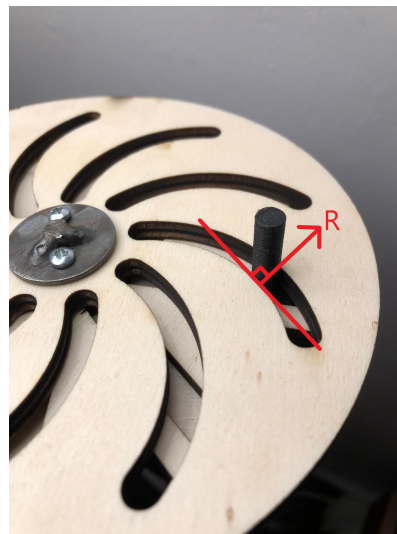


Figure 6.3: Normal force, R exerted by the upper arm to the pulley

From **Eq. 6.2**, F is the maximum frictional force, μ is the friction coefficient and R is the normal force.

$$F = \mu R \quad (6.2)$$

The higher the friction coefficient and the normal force exerted, the more friction the pins will experience against the arc of the upper arm which make it more difficult to move. We cannot change the normal force as the upper arm needs to apply a perpendicular force for the pins to move. To decrease the frictional force, we can opt for materials with a

lower friction coefficient. Since plywood and PLA have quite a high friction coefficient, the expanding pulley failed to overcome it and rotate. If our choice of materials and budget were not limited for this project, we would opt for different materials, such as: PTFE, which has a friction coefficient of 0.05 [36]. By using PTFE, we can minimize our frictional force, and, thus, the pins could move along the arc of the upper arm changing the belt's diameter as expected.

Another change that could be done to overcome the problem of having a high friction coefficient between the two surfaces could be having linear arcs in the upper arm instead of curved arcs **Figure 6.4**. By having linear arcs, the pins can be pushed out easily when the upper arm is spinning. However, by implementing linear arcs, any small rotation results in a large actuation. To deal with this large actuation, we would have to lower the resolution of actuation in the servo, i.e. one degree of servo rotation equals to 20% expansion. Another drawback of having linear arcs is that in contraction they would offer a lower resistance to belt tension. Thus, if the belt is in tension along the pins, it will contract the pulley easily. Therefore, using materials with a lower friction coefficient is likely the best strategy.

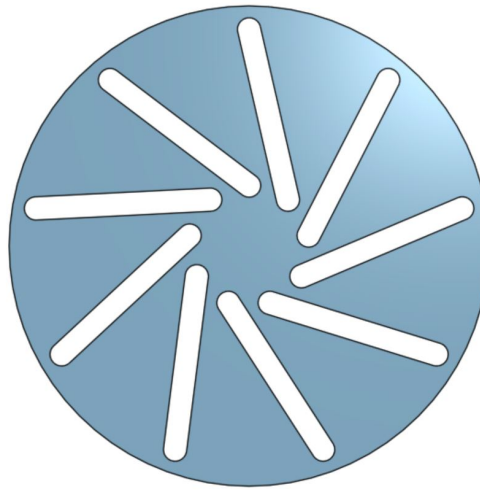


Figure 6.4: Hypothetical upper arm with linear arcs

The second improvement could be increasing the diameter of the expanding pulley to obtain a higher expansion ratio, ΔA . As we are making a direct comparison between the Hoberman ring and the expanding pulley, the size of the expanding pulley is limited to the size of Hoberman. In theory, the expansion ratio that can be achieved by the expanding pulley is infinite. In the future, we would consider designing a larger expanding pulley to have a greater expansion ratio. The belt could, therefore, change its size seamlessly, as the changing ratio is large.

6.2 Comparative Difference Between Conventional CVT, Hoberman, and Expanding Pulley

Since our two proposed mechanisms are focused on reducing the axial width in a belt-driven CVT, we will use a pulley-based CVT as a comparison to our Hoberman and expanding pulley CVT. In order to compare the pulley-based CVT, the Hoberman, and the expanding pulley, they must first have the same outer diameter to ensure for a fair comparison. Hence, the pulley-based CVT is assumed to have an outer radius of 67.5mm as this is the outer radius used to manufacture the Hoberman and the expanding pulley.

6.2.1 Expansion Ratio

The expansion ratio in conventional CVTs can vary depending on their commercial use. To ensure an unbiased comparison, we will use a pulley-based CVT that has a gear ratio of 2:1 or 1:2. This means that expansion ratio of the pulley-based CVT that will be used for this comparative analysis is 4. As seen previously in **Figure 4.12**, the Hoberman ring's expanding ratio is limited by the pushing arms, thus, having an expansion ratio of only 2. On the other hand, the expanding pulley could achieve an expansion ratio of up to 8.6 as mentioned in **Table 4.4**. Since the expanding pulley did not need pushing arms to actuate, the pins can expand and contract to the smallest diameter approaching the center. This is why the expanding pulley can attain an expansion ratio that is higher than the Hoberman.

6.2.2 Number of Parts

The pulley-based CVT is made up of four cones, the shaft and a complex hydraulic system that sums to more than 10 parts. The Hoberman is an extremely complex system that comprises over 200 small parts when including both of the Hoberman mechanisms, as described in **Section 4.6.1**. The expanding pulley, on the other hand, consists of three major parts (**Figure 4.9**). The total number of parts in the expanding pulley will be approximately 15, for one side, including the nine pins, the shaft, a bearing, and the servo-shaft coupler needed to actuate the expanding pulley. To implement the expanding pulley in a CVT, we will need two of these mechanisms which sums up to a total of 30 parts. However, the number of parts does not define the efficiency of the system. In terms of space reduction, the Hoberman which has over 200 parts had a thinner width in the axial direction compared to the pulley-based CVT.

6.2.3 Width

When it comes to space we have developed 3 governing equations that govern the axial width of the pulley-based CVT, the Hoberman, and the expanding pulley.

For the pulley-based CVT, the width, W_{cvt} is described by **Eq. 6.3**. From **Eq. 6.3**, we find that the width of the pulley-based CVT would equal to 78mm for a radius identical to

our manufactured prototypes.

$$W_{cvt} = \frac{r_{cone} \cdot 2}{\tan(90 - \sum_{Vbelt})} \quad (6.3)$$

Next, for the Hoberman, the width, W_h is described by **Eq. 6.4**. From **Eq. 6.4**, we find that the width is 65.91mm, which is supported by the caliper measurement of the prototype.

$$W_h = W_{rail} + W_{cap} + 2 \cdot (W_{scissor} + W_{arm}) \quad (6.4)$$

Lastly, the width of the expanding pulley, W_{ep} can be obtained by using **Eq. 6.5**. From **Eq. 6.5**, the expanding pulley has a width of 10.92mm, which was also confirmed by measuring the prototype.

$$W_{ep} = W_{upperarm} + W_{lowerarm} + (W_{pin} - (W_{upperarm} + W_{lowerarm})) \quad (6.5)$$

Therefore, the Hoberman is 15.5% smaller in the axial direction than the pulley-based CVT, meanwhile the expanding pulley has the largest reduction in width by being 86% smaller compared to the pulley-based CVT.

The comparative differences discussed above are summarized in **Table 6.1**.

Component Name	Unit	Pulley-based CVT	Hoberman	Expanding pulley
Expansion ratio	-	4.0	2.0	8.6
Number of parts	-	Over 10 parts	Over 200 parts	Over 30 parts
Axial width	mm	78	60	28
Space reduction	%	0 (reference)	15.5	86

Table 6.1: Comparison between pulley-based CVT, Hoberman ring, and expanding pulley

6.3 Success Aspects

At the beginning, our success in the project execution was uncertain, but the more we went forward, the more things became clear. The very first step was to check the possibility of making the project happen in a short time. We began investigating the Hoberman ring theory and checking the viability of the calculations presented in the literature. As soon as this was completed, and after several iterations, we were finally able to make the CAD models which were the first valuable indicator that we were on the right path. After this, we used a Prusa Mini 3D printer to print (using PLA filament) the different parts of the Hoberman, which came to a total of more than 200 parts. It was clear that printing the parts had been the correct choice for a complex structure like the Hoberman. Thanks to the 3D printer having a nozzle diameter of 0.4mm, small parts could be printed at a high resolution easily. During the lab sessions, the Hoberman structure was assembled piece-by-piece. This process had minor hindrances and difficulties, such as time limitations, yet we managed to finish up the build-up process in time. This was a result of good time management in our laboratory

sessions as well as good planning beforehand. Additionally, we worked efficiently by assigning each member a task in the laboratory. It is worth noting that the use of PLA was largely based on its accessibility and ease-of-use. If we had a specific application, we would adjust the material choice accordingly.

The theoretical approach for the expanding pulley was similar to the Hoberman. However, we used a laser cutter, as the 3D printer bed was not big enough for this. This approach provided more accuracy and precision than other available options. In addition, we used strong wood adhesive to stick the two wooden sheets which is superior to staplers in our case since stress concentration is undesired.

For the actuation mechanism, we believe that the implementation of the Bluetooth module resulted in a much more smooth control of the Hoberman and the expanding pulley movement. Lastly, we managed to fit the servo to actuate the Hoberman structure without affecting the Euclidean space significantly.

6.4 Further Applications of Meta-Structure CVTs

The application of meta-structure based CVTs could be revolutionary and endless. In any application where a changing gear ratio is required, meta-structure CVTs could be used to avoid the torque drop during a gear change, increase system efficiency and ultimately reduce the space that the gear mechanism consumes.

In wind turbines, the application of meta-structure CVTs would reduce the axial space that the gearbox would consume in the nacelle and would additionally avoid the torque drop. This would allow for more compact and efficient turbines as discussed in **Section 2.1.2**. Finally, the use of meta-structures in motorsports would drastically improve the efficiency and performance of the racecars by completely eliminating the torque drop.

6.5 Alternative Methods for Proving the Hypothesis

There are additional methods of proving the hypothesis that could have been implemented if time constraints had not existed. One such method would be to obtain the width measurement directly from SolidWorks. The advantage of this method is that it could be used to test the hypothesis at several different scales without having to build several models – the CAD parts and assemblies could simply be scaled up and down. Another method for proving the hypothesis would be to build both a traditional CVT and a meta-structure CVT that have the same gear expansion ratios and to perform a critical comparison between them. The advantage of this method would be that if space reduction was achieved it would be evident in the physical comparison. The disadvantage of this method is that it is more qualitative than quantitative and it would require a significant amount more design and manufacturing work.

We believe our method is quantitative and achievable in proving our hypothesis.

Chapter 7

Conclusion

In conclusion, we acknowledged the space occupancy dilemma of conventional CVTs in today's market. We began investigating our hypothesis by introducing the Hoberman ring and the expanding pulley mechanisms as meta-structures to reduce space in CVTs. Both structures were analysed through iterative processes. Then, we set up a model to examine the space reduction within the structures. That being done, we began carrying out simulations using SOLIDWORKS to further ensure the strength of our designs. After several iterations producing the optimal design, we began manufacturing the parts in the laboratory. Additive manufacturing techniques were used to provide higher precision for a small structure using PLA filament in the Hoberman ring and expanding pulley alongside the available laboratory equipment. However, the expanding pulley showed deficiency as friction played a vital role in it failing to actuate. We were able to achieve an expansion ratio of 4 for the Hoberman and 8.6 for the expanding pulley. The actuation mechanism was run by two servos and a Bluetooth module controlled by a phone to adjust the angles. Both acted in opposite directions to give rise to inverse actuation. Through discussing the results obtained after manufacturing both mechanisms, we laid out improvements on how both mechanisms can be developed for future research. Additionally, we carried out a comparative analysis between a conventional pulley-based CVT, the Hoberman ring, and the expanding pulley. For the purpose of fairness in the analysis, we used a conventional CVT with a 2:1 gear ratio. This analysis showed that the expansion ratio of conventional CVTs is 4, whilst the expansion ratios of the Hoberman and the expanding pulley were 4 and 8.6, respectively. Furthermore, the number of parts required to construct a conventional CVT is just over 10, whilst the Hoberman ring required over 200, and the expanding pulley used ± 30 . The crucial aspect of each system was their width, specifically along the shaft axis. We developed three equations to determine the axial width of the three systems. We used the conventional CVT space as a reference with a width of 78mm, determined based on the radius of our prototypes. These equations showed that the Hoberman structure reduces the axial space by 15.5%. Alternatively, the expanding pulley showed a significant reduction in the axial space of 86%. **Therefore, we can confidently ACCEPT our hypothesis that meta-structures in CVT design will reduce their Euclidean space, specifically along the shaft axis.**

References

- [1] Tian Chen, Osama R Bilal, Robert Lang, Chiara Daraio, and Kristina Shea. Autonomous deployment of a solar panel using elastic origami and distributed shape-memory-polymer actuators. *Physical Review Applied*, 11(6):064069, 2019.
- [2] Vishu Seelan. Analysis, design and application of continuously variable transmission (cvt). *Int J Eng Res Appl*, 5(3):99–105, 2015.
- [3] Ewan M Berge and A Pramanik. Analysis and material selection of a continuously variable transmission (cvt) for a bicycle drivetrain. In *Introduction to mechanical engineering*, pages 43–81. Springer, 2018.
- [4] Nilabh Srivastava and Imtiaz Haque. A review on belt and chain continuously variable transmissions (cvt): Dynamics and control. *Mechanism and machine theory*, 44(1):19–41, 2009.
- [5] Simon Ouellette and Peter Radziszewski. Design and development of a utility electric snowmobile for use in sensitive extreme environments. *Proceedings of the Canadian Engineering Education Association (CEEA)*, 2006.
- [6] Earle Buckingham. *Analytical mechanics of gears*. Courier Corporation, 1988.
- [7] Pradeep Setlur, John R Wagner, Darren M Dawson, and Bernard Samuels. Nonlinear control of a continuously variable transmission (cvt). *IEEE Transactions on control systems technology*, 11(1):101–108, 2003.
- [8] Duanling Li and Xingze Wang. Design for a kind of combined mechanisms based on gear pairs. In *2011 6th IEEE Conference on Industrial Electronics and Applications*, pages 1646–1648. IEEE, 2011.
- [9] L Mangialardi and G Mantriota. The advantages of using continuously variable transmissions in wind power systems. *Renewable Energy*, 2(3):201–209, 1992.
- [10] R Bharani and A Sivaprakasam. A review analysis on performance and classification of wind turbine gearbox technologies. *IETE Journal of Research*, pages 1–15, 2020.
- [11] Haiying Sun, Xiaoxia Gao, and Hongxing Yang. A review of full-scale wind-field measurements of the wind-turbine wake effect and a measurement of the wake-interaction effect. *Renewable and Sustainable Energy Reviews*, 132:110042, 2020.

- [12] B Bonsen, TWGL Klaassen, RJ Pulles, SWH Simons, M Steinbuch, and PA Veenhuizen. Performance optimisation of the push-belt cvt by variator slip control. *International journal of vehicle design*, 39(3):232–256, 2005.
- [13] Nilabh Srivastava and Imtiaz Haque. A review on belt and chain continuously variable transmissions (cvt): Dynamics and control. *Mechanism and machine theory*, 44(1): 19–41, 2009.
- [14] Engineering Learn. *Types of Belt Drive: Material, Applications, Advantages Disadvantages*, 2022. <https://engineeringlearn.com/types-of-belt-drive-material-applications-advantages-disadvantages/> [Accessed: 24-10-2022].
- [15] Keane Phillip. *PETG vs PLA: How do they compare?* Wevolver, 2021. <https://www.wevolver.com/article/petg-vs-pla-how-do-they-compare> [Accessed: 2022-10-16].
- [16] Facundo Arceo. *3D solved - Best 3D printing Material/filament for Gears*, 3D Solved, 2021. <https://3dsolved.com/best-3d-printing-filament-for-gears/> [Accessed: 2022-10-16].
- [17] Laxman B Abhang and Akshay Govardhan Dekhane. Use of polylactic acid (pla) material for asymmetric spur gear manufactured by 3-d printing. In *Advanced Manufacturing and Materials Science*, pages 103–113. Springer, 2018.
- [18] Mert Safak Tunalioglu and Bekir Volkan Agca. Wear and service life of 3-d printed polymeric gears. *Polymers*, 14(10):2064, 2022.
- [19] Daniel Besnea, Ciprian Rizescu, Edgar Moraru, Elena Dinu, and Iolanda Panait. Comparative study regarding the wear of gearwheels manufactured through additive technologies. In *MATEC Web of Conferences*, volume 290, page 08001. EDP Sciences, 2019.
- [20] Robert Fischer, Ferit Küçükay, Gunter Jürgens, Rolf Najork, and Burkhard Pollak. Transmission designs for passenger cars. In *The Automotive Transmission Book*, pages 229–273. Springer, 2015.
- [21] Andres Garcia. *What is Flat Belt Drive? — Its Advantages and Disadvantages.*, 2019. <https://mechathon.com/flat-belt-drive/> [Accessed: 24-10-2022].
- [22] Guillaume Rivière Maxime Daniel and Nadine Couture. Designing an expandable illuminated ring to build an actuated ring chart. *Embedded, and Embodied Interaction*, 1(1): 140–145, 2018.
- [23] Maya Pishvar and Ryan L Harne. Foundations for soft, smart matter by active mechanical metamaterials. *Advanced Science*, 7(18):2001384, 2020.

- [24] Xiaoguang Zhao, Guangwu Duan, Aobo Li, Chunxu Chen, and Xin Zhang. Integrating microsystems with metamaterials towards metadevices. *Microsystems & nanoengineering*, 5(1):1–17, 2019.
- [25] Shuai Wu, Qiji Ze, Rundong Zhang, Nan Hu, Yang Cheng, Fengyuan Yang, and Ruike Zhao. Symmetry-breaking actuation mechanism for soft robotics and active metamaterials. *ACS applied materials & interfaces*, 11(44):41649–41658, 2019.
- [26] Rui-Jia Xu and Yu-Sheng Lin. Actively mems-based tunable metamaterials for advanced and emerging applications. *Electronics*, 11(2):243, 2022.
- [27] Bruno Grossi, H Palza, JC Zagal, C Falcón, and G During. Metarpillar: Soft robotic locomotion based on buckling-driven elastomeric metamaterials. *Materials & Design*, 212:110285, 2021.
- [28] Yichao Tang, Yanbin Li, Yaoye Hong, Shu Yang, and Jie Yin. Programmable active kirigami metasheets with more freedom of actuation. *Proceedings of the National Academy of Sciences*, 116(52):26407–26413, 2019.
- [29] Daniela Rus Ryan L. Truby, Lillian Chin. A recipe for electrically-driven soft robots via 3d printed handed shearing auxetics. *ieeexplore*, 6:795–802, 2021.
- [30] Lerner E Brandenbourger M., Locsin X. Non-reciprocal robotic metamaterials. *Nature*, (4608):795–802, 2019.
- [31] M.Srinivasanb Ashok KumarNallathambiaC, Lakshmana RaobSivakumar. Large deflection of constant curvature cantilever beam under follower load. *International Journal of Mechanical Sciences*, 52:440–445, 2009.
- [32] Anubha Parashar. Design and autonomous control of the active adaptive suspension system rudra – mars rover. 2013.
- [33] Kyoungwoo Park Byeong-Sam Kim. Dkinematic motion analysis and structural analysis of bellcrank structures using fem. 2013.
- [34] B. Ya. Sacheka and A. M. Mezrin. Studies on the tribological characteristics of euro-pallets on film-faced plywood. *Journal of Friction and Wear*, 41:277–281, 2020.
- [35] A. Altinkaynak S.Z. Hervan and Z. Parlar. Hardness, friction and wear characteristics of 3d-printed pla polymer. *Journal of Engineering Tribology*, 235:1590–1598, 2020.
- [36] S Bahadur. Friction of polymers. *Encyclopedia of Tribology*, pages 1365–1372, 2013.

Appendix A

Electronic Supplementary Material

A.1 Experimental Hoberman Videos

S1: <https://youtu.be/QiqGmfRHzzjQ> - This video shows how the Hoberman expansion was measured experimentally.

S2: <https://youtu.be/vtC3A1jAGXg> - This video shows both Hoberman rings expanding and contracting.

A.2 Hoberman Arduino Code

S3: <https://github.com/rodrigocarnero/Hoberman-CVT-Arduino-Code> - This is the Arduino code on GitHub, which was used to enable Bluetooth connection and control of the servos to actuate the Hoberman.

A.3 Simulation Supplementary material

S4: https://drive.google.com/drive/folders/12pyePH-ji_LB6Mm4lu6B07kKAQ0SbnY1?usp=sharing - All files retaining the raw outputs of the simulations and optimization

A.4 Hoberman CAD Files

S5: <https://drive.google.com/drive/folders/1jY6QCtlRnzKiby8y9JWwSQEMF3ZjUsSx?usp=sharing> - All Hoberman ring CAD files used in simulation and optimization

A.5 Experimental Expanding Pulley Videos

S6: <https://youtu.be/F5uIKEMy5Is> - This video shows the animation of the expanding pulley expanding and contracting in OnShape

S7: <https://youtube.com/shorts/v2tOs-YL9JE?feature=share> - This video shows the failed actuation of the manufactured expanding pulley

A.6 Expanding Pulley CAD Files

S8: https://drive.google.com/drive/folders/1vpAAtNn4m6HDK_F3VNw5HW3yt3oUOOho?usp=sharing - All expanding pulley CAD files

Appendix B

Hoberman Iteration Calculations

B.1 Iteration 1:

Reasoning behind the chosen values explained in **Section 4.2**.

1. $n = 18$
2. $w = 5$
3. $\Delta A_{Outer} = 10$
4. $r_{max} = 67.5\text{mm}$

From **Eq. 4.2**, we rearrange to make r_{min} the subject.

$$r_{min} = \frac{r_{max}}{\sqrt{\Delta A_{Outer}}} = \frac{67.5}{\sqrt{10}} = 21.3\text{mm} \quad (\text{B.1})$$

From **Eq. 4.7**.

$$\alpha_{max} = \frac{\pi}{2} - \frac{\pi}{n} = \frac{\pi}{2} - \frac{\pi}{18} = 1.4\text{rad} \quad (\text{B.2})$$

From **Eq. 4.8**, we rearrange to make $r_{inner@collapsed}$ the subject.

$$r_{inner@collapsed} = \frac{w}{2} \cdot \sin \alpha_{max} = \frac{5}{2} \cdot \sin 1.4 = 2.5\text{mm} \quad (\text{B.3})$$

From **Eq. 4.10**

$$r_{inner@expanded} = r_{max} - w = 67.5 - 5 = 62.5\text{mm} \quad (\text{B.4})$$

From **Eq. 4.6**, we rearrange to make L the subject.

$$L = \frac{r_{min} - r_{inner@collapsed}}{2 \cdot \sin \alpha_{max}} = \frac{21.3 - 2.5}{2 \cdot \sin 1.4} = 9.6\text{mm} \quad (\text{B.5})$$

B.2 Iteration 2:

Reasoning behind the chosen values explained in **Section 4.2**.

1. $n = 12$
2. $w = 10$
3. $\Delta A_{Outer} = 5$
4. $r_{max} = 67.5mm$

From **Eq. 4.2**, we rearrange to make r_{min} the subject.

$$r_{min} = \frac{r_{max}}{\sqrt{\Delta A_{Outer}}} = \frac{67.5}{\sqrt{5}} = 30.2mm \quad (B.6)$$

From **Eq. 4.7**.

$$\alpha_{max} = \frac{\pi}{2} - \frac{\pi}{n} = \frac{\pi}{2} - \frac{\pi}{12} = 1.31rad \quad (B.7)$$

From **Eq. 4.8**, we rearrange to make $r_{inner@collapsed}$ the subject.

$$r_{inner@collapsed} = \frac{w}{2} \cdot \sin \alpha_{max} = \frac{10}{2} \cdot \sin 1.31 = 4.8mm \quad (B.8)$$

From **Eq. 4.10**

$$r_{inner@expanded} = r_{max} - w = 67.5 - 10 = 57.5mm \quad (B.9)$$

From **Eq. 4.6**, we rearrange to make L the subject.

$$L = \frac{r_{min} - r_{inner@collapsed}}{2 \cdot \sin \alpha_{max}} = \frac{30.2 - 4.8}{2 \cdot \sin 1.31} = 13.1mm \quad (B.10)$$

B.3 Iteration 3:

Reasoning behind the chosen values explained in **Section 4.2**.

1. $n = 8$
2. $w = 10$
3. $\Delta A_{Outer} = 1.8$
4. $r_{max} = 67.5mm$

From **Eq. 4.2**, we rearrange to make r_{min} the subject.

$$r_{min} = \frac{r_{max}}{\sqrt{\Delta A_{Outer}}} = \frac{67.5}{\sqrt{1.8}} = 50.3mm \quad (B.11)$$

From **Eq. 4.7.**

$$\alpha_{max} = \frac{\pi}{2} - \frac{\pi}{n} = \frac{\pi}{2} - \frac{\pi}{8} = 1.18 \text{ rad} \quad (\text{B.12})$$

From **Eq. 4.8**, we rearrange to make $r_{inner@collapsed}$ the subject.

$$r_{inner@collapsed} = \frac{w}{2} \cdot \sin \alpha_{max} = \frac{10}{2} \cdot \sin 1.18 = 4.6 \text{ mm} \quad (\text{B.13})$$

From **Eq. 4.10**

$$r_{inner@expanded} = r_{max} - w = 67.5 - 10 = 57.5 \text{ mm} \quad (\text{B.14})$$

From **Eq. 4.6**, we rearrange to make L the subject.

$$L = \frac{r_{min} - r_{inner@collapsed}}{2 \cdot \sin \alpha_{max}} = \frac{50.3 - 4.6}{2 \cdot \sin 1.18} = 24.7 \text{ mm} \quad (\text{B.15})$$

Appendix C

Expanding Pulley

C.1 Iteration 1:

In **Section 4.4**, the values obtained in **Table 4.2** are calculated using **Eq. 4.14**. The width of arc are kept constant throughout the iteration process which is 6mm. The calculations obtained are shown below.

$$\Delta A = \left[\frac{r_{\text{maximum@expanded}}}{r_{\text{minimum@contracted}}} \right]^2 = \left[\frac{60.0}{14.9} \right]^2 = 16.2 \quad (\text{C.1})$$

C.2 Iteration 2:

The same calculations are repeated for the second iteration using the same equation as in iteration 1. The width of arc used is 6mm. The calculations obtained are shown below.

$$\Delta A = \left[\frac{r_{\text{maximum@expanded}}}{r_{\text{minimum@contracted}}} \right]^2 = \left[\frac{60.0}{42.6} \right]^2 = 2.0 \quad (\text{C.2})$$

C.3 Iteration 4:

In the last iteration for our expanding pulley described in **Section 4.4**, using **Eq. 4.14**, the calculations to obtain the values in **Table 4.2** are shown below.

$$\Delta A = \left[\frac{r_{\text{maximum@expanded}}}{r_{\text{minimum@contracted}}} \right]^2 = \left[\frac{60.0}{20.5} \right]^2 = 8.6 \quad (\text{C.3})$$

Appendix D

Hoberman Arms Deflection Derivation

D.1 Vertical deflection of a half a circle

We will now calculate the vertical deflection of the semi-circular arm as a function of the Load P (Belt tension). We will first calculate the second moment of area of the arm as we will need it to calculate the deflection. The surface area of the arm is a rectangle as seen in **Figure D.1**. We can say that the height h is the thickness of the arm and the base b is the width of the arm. We can use the second moment of area equation of a rectangular surface area to calculate I (**Eq. D.1**).

$$I = \frac{1}{12} \cdot b \cdot h^3 = \frac{1}{12} \cdot b \cdot t^3 \quad (\text{D.1})$$

Now we will use Castigliano's first theorem. We will only consider bending stresses.

$$U_{\text{Bending}} = \int_0^{\pi} \frac{M_{\theta}^2}{2EI} ds \quad (\text{D.2})$$

But we need to convert **Eq. D.2** in polar coordinates. $ds = R d\theta$.

$$U_{\text{Bending}} = \int_0^{\pi} \frac{M_{\theta}^2}{2EI} \cdot R d\theta \quad (\text{D.3})$$

Looking at the diagram in **Figure D.2**, we can find the bending moments about any position θ . We find **Eq. D.4**.

$$M_{\theta} = P \cdot R \cdot \sin \theta \quad (\text{D.4})$$

If we take the partial derivative of **Eq. D.4**.

$$\frac{\partial M_\theta}{\partial P} = R \cdot \sin \theta \quad (\text{D.5})$$

If we now take the partial derivative of U in **Eq. D.3**, we find the vertical deflection.

$$\delta_v = \frac{\partial U_{\text{Bending}}}{\partial P} = \int_0^\pi \frac{M_\theta}{EI} \cdot \frac{\partial M_\theta}{\partial P} \cdot R d\theta \quad (\text{D.6})$$

If we substitute **Eq. D.4** and **Eq. D.5** into **Eq. D.6**, we find:

$$\delta_v = \frac{\partial U_{\text{Bending}}}{\partial P} = \frac{P \cdot R^3}{EI} \int_0^\pi \sin^2 \theta d\theta = \frac{P \cdot R^3}{EI} \cdot \left[\frac{\theta}{2} - \frac{\sin 2\theta}{4} \right]_0^\pi \quad (\text{D.7})$$

Hence vertical deflection is:

$$\delta_v = \frac{P \cdot R^3 \cdot \pi}{2 \cdot EI} \quad (\text{D.8})$$

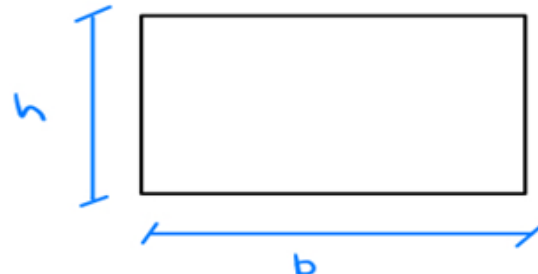


Figure D.1: Cross section of bent arm

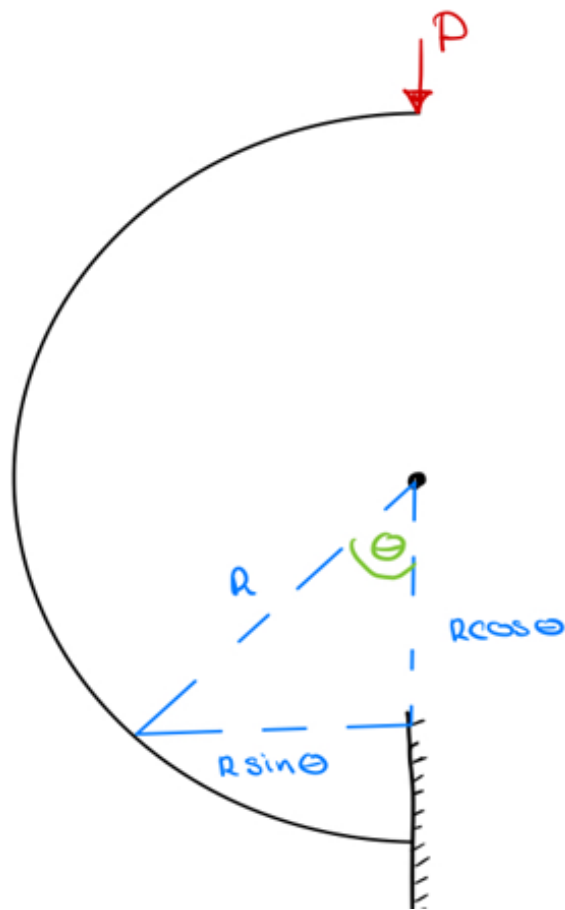


Figure D.2: FBD of bent arm

Appendix E

Arduino Circuit

E.1 Arduino Circuit Diagram

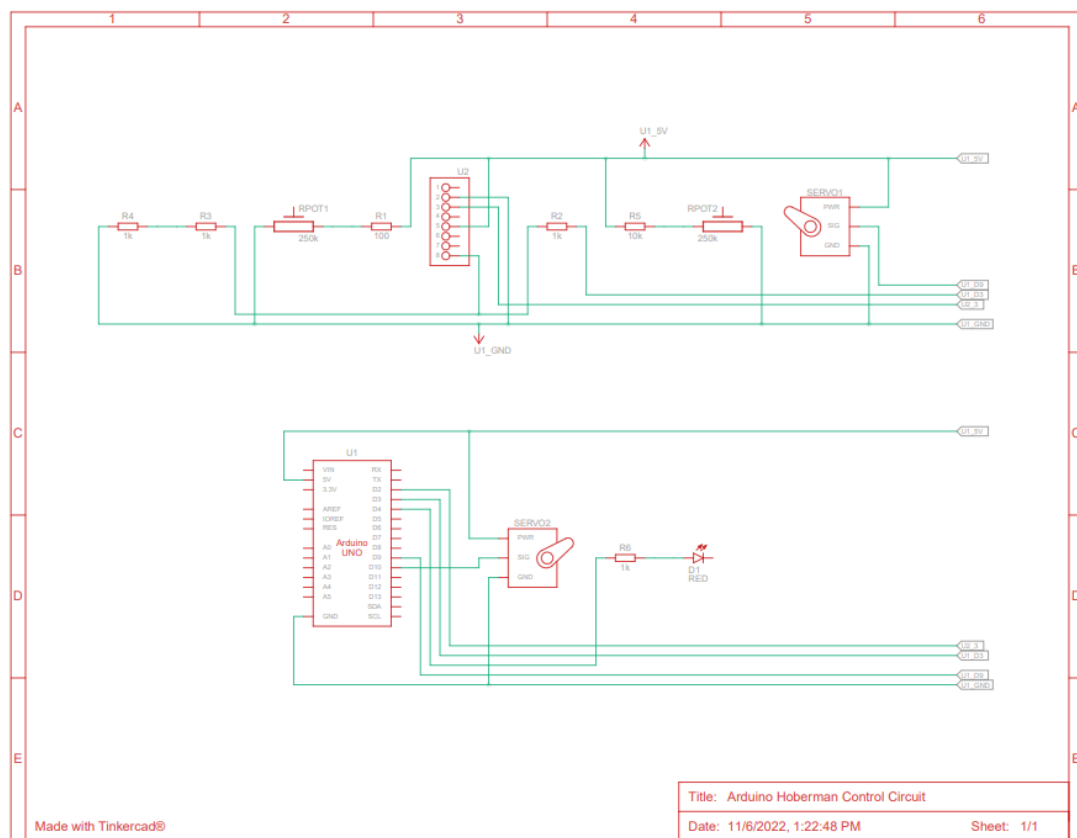


Figure E.1: Arduino circuit diagram

E.2 Potential Divider Circuit

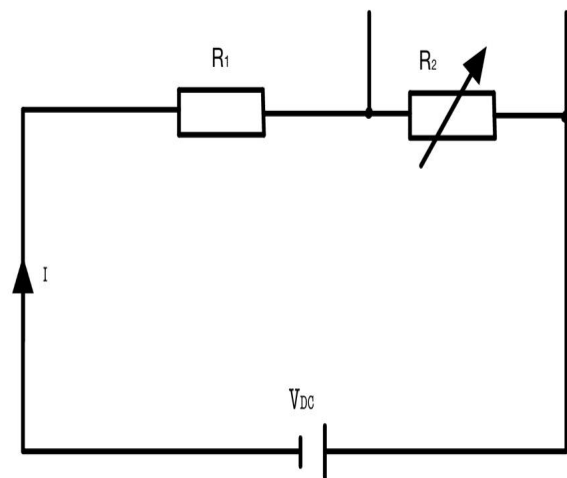


Figure E.2: Potential divider circuit

Appendix F

Bill of Materials

Product description	Sub-system	Off the shelf or manufactured	Price	Quantity	Total Price	Supplier
RC Servo MG996R (2 pieces)	Electrical	Off the shelf	£13.99	1	£13.99	Amazon
Arduino Uno R3	Electrical	Off the shelf	-	1	-	Rodrigo's
Plywood 3mm	Expanding pulley	Manufactured	£1.50	1	£1.50	G20 Lab
Plywood 6mm	Hoberman & Expanding pulley	Manufactured	£1.50	2	£3.00	G20 Lab
ø6mm x 2.4mm thick steel disc plate	Expanding pulley	Off the shelf	£1.00	1	£1.00	G20 Lab
PLA Filament 1.75mm 3D Printer	Hoberman & Expanding pulley	Off the shelf	-	1	-	Martin's
Bearing øInner 6mm x øOuter 19mm	Hoberman & Expanding pulley	Off the shelf	£2.42	5	£12.10	G20 Lab
Threaded steel ø6mm x 100mm Shaft	Hoberman & Expanding pulley	Manufactured	£0.30	2	£0.60	G20 Lab
G-Clamp 6"	Hoberman	Off the shelf	£7.99	1	£7.99	Screwfix
Draper 38267 Bench Vice, 75mm, Blue	Hoberman	Off the shelf	£16.25	0	£16.25	Amazon
Large Elastic Bands 100 Pieces, 8 inch	Hoberman	Off the shelf	£8.99	0	£8.99	Amazon
				Total	£65.42	

Table F.1: Bill Of Materials (BOM)

Appendix G

Simulations

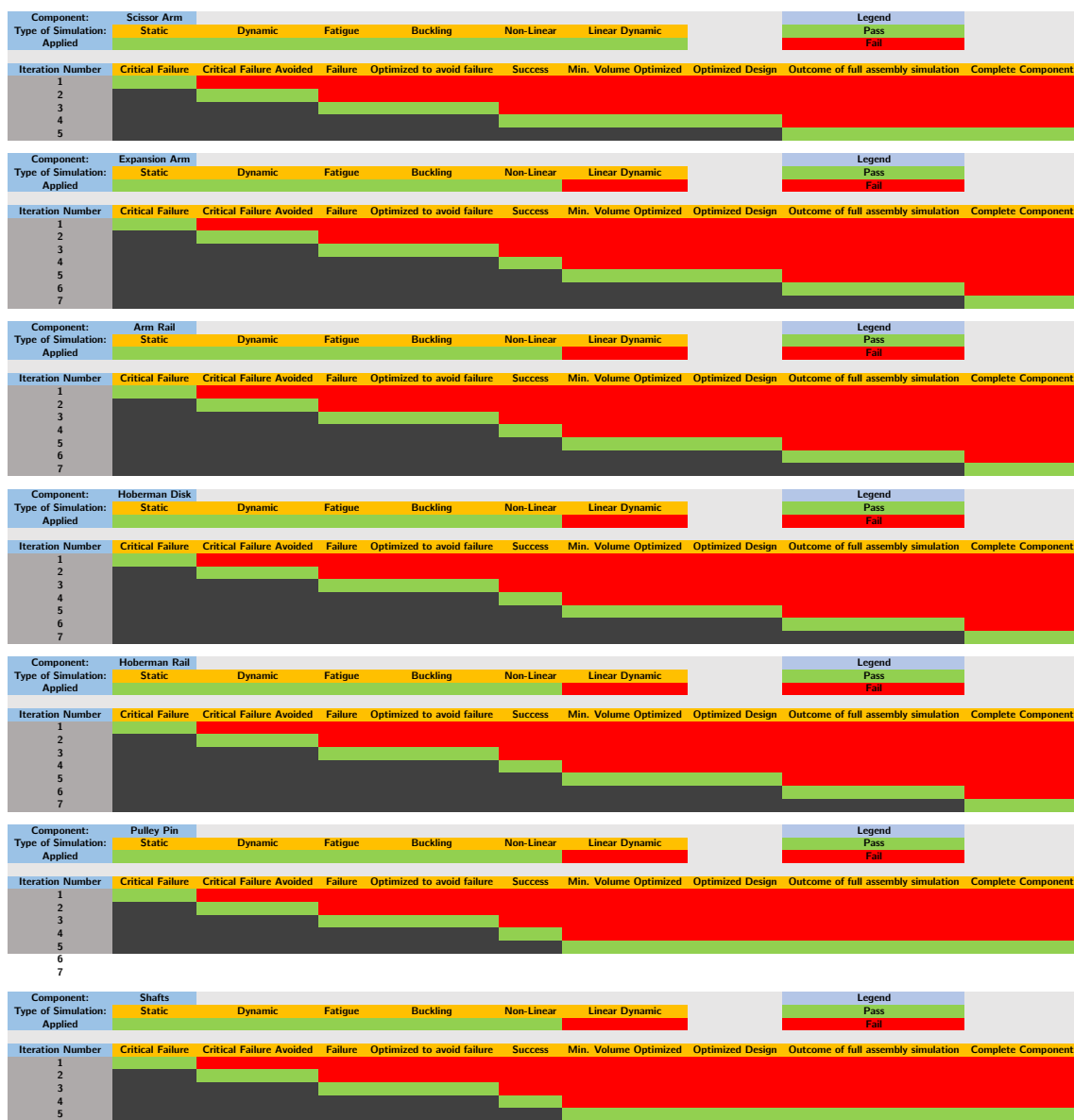


Table G.1: Optimization outcomes based of iterations and requirements